RESEARCH ARTICLE

An *In Vivo* CRISPR Screening Platform for Prioritizing Therapeutic Targets in AML

Shan Lin[1,2], Clément Larrue[3], Nastassja K. Scheidegger[1,2], Bo Kyung A. Seong[1,2], Neekesh V. Dharia[1,2], Miljan Kuljanin[4], Caroline S. Wechsler[1], Guillaume Kugener[2], Amanda L. Robichaud[1], Amy Saur Conway[1], Thelma Mashaka[5], Sarah Mouche[3], Biniam Adane[1,2], Jeremy A. Ryan[5], Joseph D. Mancias[4], Scott T. Younger[2], Federica Piccioni[2], Lynn H. Lee[6,7], Mark Wunderlich[8], Anthony Letai[2,5], Jérôme Tamburini[3], and Kimberly Stegmaier[1,2]

ABSTRACT CRISPR–Cas9-based genetic screens have successfully identified cell type–dependent liabilities in cancer, including acute myeloid leukemia (AML), a devastating hematologic malignancy with poor overall survival. Because most of these screens have been performed *in vitro* using established cell lines, evaluating the physiologic relevance of these targets is critical. We have established a CRISPR screening approach using orthotopic xenograft models to validate and prioritize AML-enriched dependencies *in vivo*, including in CRISPR-competent AML patient-derived xenograft (PDX) models tractable for genome editing. Our integrated pipeline has revealed several targets with translational value, including *SLC5A3* as a metabolic vulnerability for AML addicted to exogenous myo-inositol and *MARCH5* as a critical guardian to prevent apoptosis in AML. MARCH5 repression enhanced the efficacy of BCL2 inhibitors such as venetoclax, further highlighting the clinical potential of targeting *MARCH5* in AML. Our study provides a valuable strategy for discovery and prioritization of new candidate AML therapeutic targets.

SIGNIFICANCE: There is an unmet need to improve the clinical outcome of AML. We developed an integrated *in vivo* screening approach to prioritize and validate AML dependencies with high translational potential. We identified *SLC5A3* as a metabolic vulnerability and *MARCH5* as a critical apoptosis regulator in AML, both of which represent novel therapeutic opportunities.

[1]Department of Pediatric Oncology, Dana-Farber Cancer Institute and Boston Children's Hospital, Boston, Massachusetts. [2]The Broad Institute of MIT and Harvard, Cambridge, Massachusetts. [3]Translational Research Centre in Onco-hematology, Faculty of Medicine, University of Geneva, Geneva, Switzerland. [4]Department of Radiation Oncology, Dana-Farber Cancer Institute, Boston, Massachusetts. [5]Department of Medical Oncology, Dana-Farber Cancer Institute, Boston, Massachusetts. [6]Division of Oncology, Cancer and Blood Disease Institute, Cincinnati Children's Hospital Medical Center, Cincinnati, Ohio. [7]Department of Pediatrics, University of Cincinnati College of Medicine, Cincinnati, Ohio. [8]Division of Experimental Hematology and Cancer Biology, Cancer and Blood Disease Institute, Cincinnati Children's Hospital Medical Center, Cincinnati, Ohio.

Note: Supplementary data for this article are available at Cancer Discovery Online (http://cancerdiscovery.aacrjournals.org/).

C. Larrue and N.K. Scheidegger contributed equally to this article.

Current address for F. Piccioni: Merck Research Laboratories, Boston, Massachusetts.

Corresponding Author: Kimberly Stegmaier, Dana-Farber Cancer Institute, 450 Brookline Avenue, Boston, MA 02215. Phone: 617-632-4438; E-mail: Kimberly_stegmaier@dfci.harvard.edu

Cancer Discov 2022;12:432–49

doi: 10.1158/2159-8290.CD-20-1851

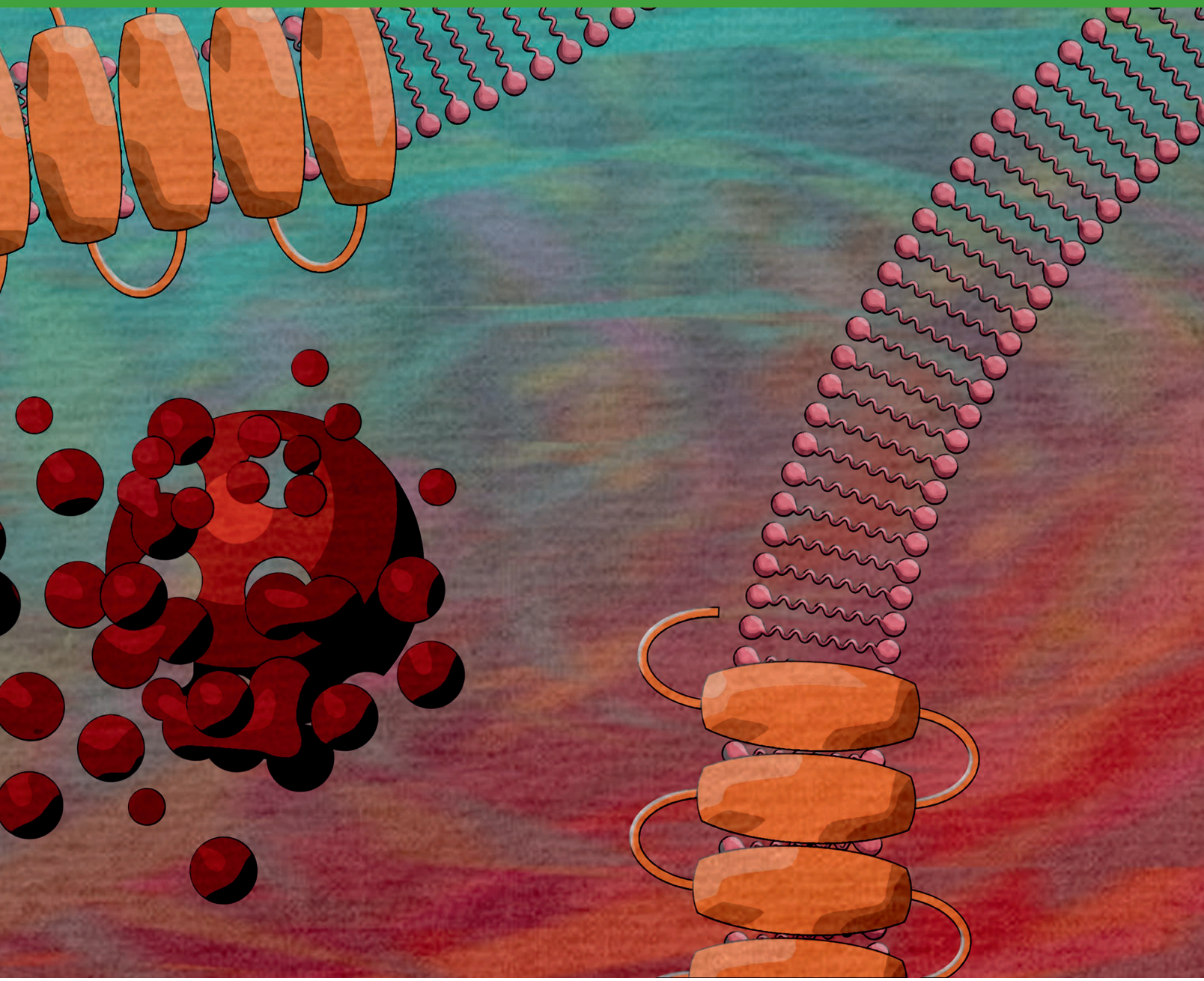

INTRODUCTION

Acute myeloid leukemia (AML) is a heterogeneous hematologic malignancy characterized by the accumulation of abnormal myeloblasts. Despite the efficacy of chemotherapy and stem cell transplantation for some patients, cure rates for AML remain between 35% and 40% overall and less than 15% for older adults (1). Continued efforts are needed to identify new therapeutic strategies for these patients.

The successful adaptation of CRISPR–Cas9 approaches for genetic screens has become a powerful tool for the unbiased discovery of essential genes in mammalian cells (2, 3). First-generation, large-scale functional genomic screens to identify the critical genes involved in cancer cell maintenance have been completed, such as the Broad Institute's and Sanger Center's Cancer Dependency Maps (DepMap; https://depmap.org/; refs. 4, 5). These efforts have revealed hundreds of potential genetic vulnerabilities in AML cells *in vitro*. How to distinguish candidates with the highest translational potential, however, remains a challenge. Therefore, a secondary functional validation approach is necessary to prioritize those gene targets for therapeutic targeting to guide the development of new antileukemia treatments.

These large-scale genetic screens were primarily performed *in vitro*. Thus, one important consideration in prioritizing candidate genes is to evaluate their essentiality in a proper *in vivo* microenvironment because the niche may influence the physiologic behavior of cancer cells. Human AML orthotopic

disease modeling is highly physiologically relevant, as AML cells will engraft in the bone marrow microenvironment in the mouse. *In vivo* CRISPR screening has been performed to identify tumor growth modulators in several genetically engineered mouse models of hematologic malignancies (6–8). However, the feasibility of such an application in human AML orthotopic xenograft models has not been demonstrated. Therefore, we optimized a protocol for CRISPR screening in orthotopic xenograft models to enable the systematic evaluation of the physiologic relevance of top AML dependencies emerging from genome-scale CRISPR–Cas9 *in vitro* screens.

Established AML cell lines are amenable to genome-scale screens; however, they cannot fully recapitulate all pathophysiologic aspects of the disease. Target validation directly in primary patient samples is desirable yet not readily accessible. Instead, the AML patient-derived xenograft (PDX) has emerged as a valuable preclinical model that largely reflects the molecular and phenotypic characteristics of the primary disease (9, 10). To interrogate the translational relevance of the targets identified from established cell lines, we developed AML PDX models amenable to genome editing. By combining *in vivo* screening and CRISPR-competent PDX models, we devised an integrated pipeline to prioritize AML dependencies and investigated the top novel targets emerging from this approach.

RESULTS

In Vivo CRISPR Screens Using Xenograft Models of Human AML

To identify AML-enriched dependency genes, we explored the DepMap Avana CRISPR–Cas9 screen dataset and selected the genes that AML cells are more dependent on for growth compared with the other cancer types included in the screen. This gene set was intersected with additional AML *in vitro* screen datasets, including the combined Broad Institute and Novartis short hairpin RNA (shRNA) screens and a focused *in vitro* CRISPR screen in AML cell lines (11, 12). These 200 top-ranked AML-enriched gene dependencies were involved in various biological pathways, such as chromatin and transcriptional regulation, metabolism, and mitochondria organization (Supplementary Fig. S1A and S1B). To distinguish the on-target from off-target antiproliferative effects caused by CRISPR-mediated DNA cutting in amplified regions (13, 14), we designed three targeting single-guide RNAs (sgRNA) and three intronic control sgRNAs for each gene. With 120 additional negative control sgRNAs, a focused library with 1,320 sgRNAs was constructed (Fig. 1A).

To better evaluate the therapeutic potential of candidate genes, we sought to investigate their *in vivo* essentiality not only in established AML cell lines but also in PDX models, argued to be the most faithful to primary human disease (11). CRISPR-mediated genetic studies in PDXs have been challenging due to the poor transduction efficiency and limited growth *in vitro*. To develop PDX models that are tractable for CRISPR editing, we screened a cohort of PDX samples and identified those transducible and suitable for short-term *in vitro* culture (Supplementary Table S1). These PDX cells were transduced with lentivirus coexpressing Cas9 and a fluorescent protein (GFP or mCherry). Cas9-expressing PDX cells were purified based on fluorescence and expanded via serial transplantation into immunodeficient NSGS (NOD scid gamma SGM3) mice (Supplementary Fig. S2A and S2B). Cas9 activity was assessed using a fluorescent protein (mAmetrine)–linked sgRNA targeting *CD33*. More than 80% of PDX cells receiving the sgRNA became CD33 negative, indicating that a high Cas9 activity can be achieved in these models (Supplementary Fig. S2C).

Next, to ensure sufficient library representation *in vivo*, we optimized the screening conditions through barcoding experiments using a library of 3,152 barcodes. Five to 10 million barcoded MV4-11 cells were injected via tail vein into NSGS mice. Sublethal irradiation was necessary for improved barcode representation in bone marrow and reduced mouse-to-mouse variation (Supplementary Fig. S2D and S2E). Although the barcode distribution was skewed in individual mice, even with irradiation, a complete and balanced library representation could be recovered by combining readouts from multiple mice (Supplementary Fig. S2F and S2G).

With all conditions optimized, we then performed parallel *in vivo* and *in vitro* screens using Cas9-expressing MV4-11 and U937 cell lines, as well as PDX16-01(CALM–AF10 fusion, *NF1*, *PHF6*, and *TP53* mutations; Fig. 1B). AML cells were transduced with the screen library in duplicate and selected for 2 days with puromycin when an aliquot of cells was collected as the input reference. We then injected 10 million cells per mouse by tail vein into four to five irradiated mice per replicate and in parallel cultured an aliquot of cells from each replicate *in vitro*. *In vitro* cultures were harvested 2 (for MV4-11) or 3 (for U937 and PDX16-01) weeks later, and the bone marrow and spleens were collected when the mice displayed signs of overt disease, such as hindlimb paralysis and dyspnea, with high leukemic engraftment (Supplementary Fig. S3A and S3B). There was strong replicate reproducibility for both the *in vitro* and *in vivo* results, although the data generated from U937 displayed a smaller dynamic range likely due to weaker Cas9 activity (Supplementary Fig. S3C). The average relative abundance of each sgRNA in the output compared with the input samples was determined. Both the abundance and depletion of individual sgRNA in the bone marrow versus the spleen were strongly correlated (Fig. 1C; Supplementary Fig. S3D); therefore, we focused on the bone marrow data for the downstream analysis.

We calculated a normalized depletion score for each sgRNA (see Supplementary Methods and Supplementary Table S2). The median value of each set of three sgRNAs was used to represent the score of the corresponding gene. Using the intronic guide population as a null distribution, we defined hits for each model (Supplementary Table S3). *In vitro* and *in vivo* hits were generally well correlated. However, a modest number of targets did not score well *in vivo*, with a few targets displaying *in vitro* versus *in vivo* discrepancies in multiple models (Supplementary Fig. S3E and S3F). These results underscore the importance of an *in vivo* validation strategy for refining the hits emerging from a primary *in vitro* screen. Notably, many genes were confirmed as hits in PDX16-01 *in vivo* and overlapped with those validating in the MV4-11 and U937 models (Fig. 1D), lending support to the relevance of using AML cell lines for dependency identification. Gene Ontology analysis showed an enrichment of metabolism- and

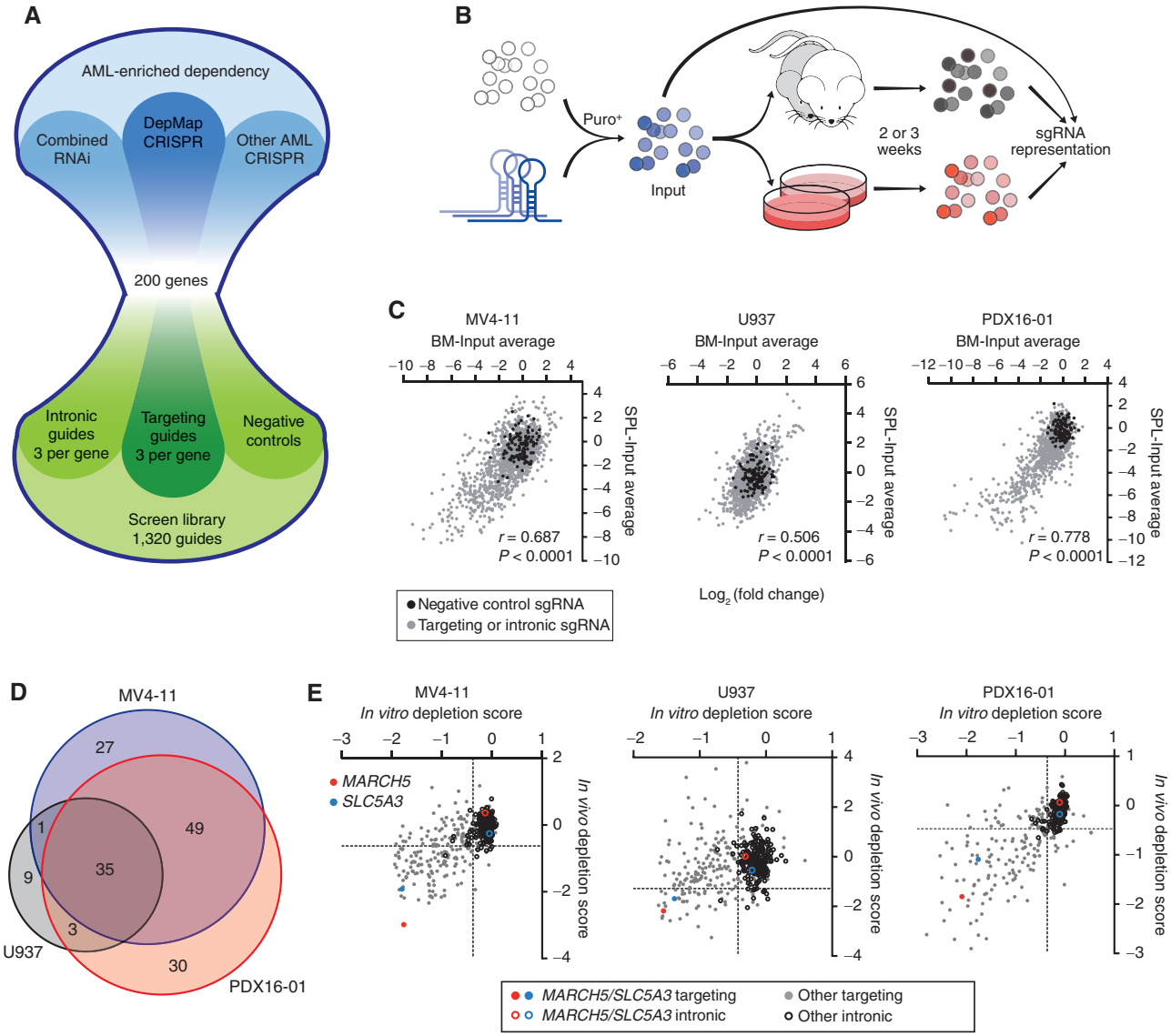

Figure 1. *In vivo* CRISPR screens prioritize genetic dependencies in human AML. **A,** Schematic of the library design. **B,** Schematic of *in vitro* and *in vivo* CRISPR screening approach. **C,** Scatter plots showing the correlation of relative abundance of sgRNAs in bone marrow (BM) versus spleen (SPL). Data points representing negative control sgRNAs (black solid circles) are indicated. **D,** Venn diagram showing the number of *in vivo* hits scoring in bone marrow of each AML model. **E,** Scatter plots showing the *in vitro* and *in vivo* depletion scores of *SLC5A3* and *MARCH5* at a gene level in three AML models. Data points representing the median value of each intronic sgRNA set are indicated (black hollow circles). Scores of *SLC5A3* and *MARCH5* (blue and red solid circles) and their intronic controls (blue and red hollow circles) are highlighted.

mitochondria-associated pathways in all three models (Supplementary Fig. S4A and S4B), consistent with recent findings that AML cells rely on unique metabolic and mitochondrial properties for survival (15, 16). In addition, several hematopoietic lineage–related transcription factors appeared to be strong *in vivo* dependencies (Supplementary Fig. S4C), corroborating recent studies targeting transcriptional vulnerabilities in AML (17, 18). Further supporting the validity of our screen, the transcription factors *KMT2A* (also called *MLL*, *mixed lineage leukemia* gene) and *ZFP64* specifically scored in MV4-11, which is driven by an MLL fusion oncogene. *ZFP64* is required to sustain expression of this fusion (Supplementary Fig. S4C; ref. 19). Altogether, our screen provided an informative list of AML targets with high physiologic relevance (Supplementary Table S3).

Next, we focused on targets that previously had not been described as AML dependencies and ranked highly as *in vivo* hits in all three models in the bone marrow: the sodium/myo-inositol cotransporter *SLC5A3* and the mitochondria-localized RING-type ubiquitin E3 ligase *MARCH5* (Fig. 1E; Supplementary Fig. S5A; refs. 20, 21). *SLC5A3* and *MARCH5* also displayed strong depletion scores in the data from spleen in the MV4-11 and PDX16-01 models and a modest depletion score in the U937 model (Supplementary Fig. S5B). We re-mined the latest edition of the DepMap CRISPR screening datasets, which continue to be expanded, and confirmed that

SLC5A3 and *MARCH5* were indeed strong dependencies in most AML cell lines, displaying a more essential role in AML compared with other cancer types (Supplementary Fig. S5C; Supplementary Table S4). We therefore selected these two targets for further validation as novel therapeutic opportunities for AML.

SLC5A3 Is Required for Sustaining AML Growth

SLC5A3 belongs to the solute carrier family, and among all five solute carrier family members included in our screen library, *SLC5A3* was the top scoring (Supplementary Fig. S6A). We validated this dependency in several AML cells lines and PDX models using two independent *SLC5A3*-targeting sgRNAs. *SLC5A3* depletion suppressed the growth of AML cells as demonstrated by an *in vitro* competition assay (Fig. 2A and B). As a validated SLC5A3 antibody was unavailable, we confirmed the genomic editing of the *SLC5A3* locus by Sanger sequencing and the Inference of CRISPR Edits (ICE) analysis, with a high editing efficiency achieved (Supplementary Fig. S6B–S6D). The on-target effect was further supported by using a CRISPR-resistant *SLC5A3* cDNA to rescue the growth defect (Fig. 2C). The cellular alterations after *SLC5A3* deletion were examined. Interestingly, SLC5A3 inhibition disturbed cell-cycle distribution in a cell context–dependent manner, including reduced S phase and increased sub-G1, G1/G0, or G2 phase (Supplementary Fig. S6E). SLC5A3 depletion did not promote obvious differentiation, as assessed by CD11b staining, except for PDX17-14 (MLL–AF10 fusion), which displayed an upregulation of CD11b expression associated with morphology changes consistent with differentiation (Supplementary Fig. S6F and S6G). By contrast, an upregulation of Annexin V and cleaved caspase 3 levels was consistently observed in all AML models tested, indicating that apoptotic cell death is a common consequence of SLC5A3 disruption (Fig. 2D and E).

We next asked whether disruption of SLC5A3 posttransplantation can repress AML progression *in vivo*. PDX16-01 cells were transduced with a doxycycline-inducible CRISPR vector coexpressing GFP (22). Purified GFP^+ cells were transplanted into NSGS mice, and the nontargeting control or *SLC5A3*-targeting sgRNA was induced 1 week later by serving a doxycycline-containing diet (Fig. 2F). Compared with the control group, mice receiving *SLC5A3*-knockout cells displayed significantly reduced leukemic burden as evaluated by bone marrow aspiration, as well as prolonged survival (Fig. 2G and H). Notably, a subset of the leukemia cells from the *SLC5A3*-knockout group was GFP negative at the time of disease progression, which was not observed in the control group (Supplementary Fig. S6H and S6I). In accordance, ICE analysis showed that only a minor population of these cells retained *SLC5A3* locus editing (Supplementary Fig. S6J). Therefore, it is likely that AML cells escaping from *SLC5A3* deletion outgrew and contributed to leukemia progression, emphasizing the essential role of SLC5A3 for AML progression *in vivo*.

SLC5A3 Transports Myo-inositol to Support AML Cell Proliferation

Myo-inositol and its derivatives are involved in several cellular processes. Because SLC5A3 is one of the major myo-inositol transporters, we investigated whether the growth defect caused by SLC5A3 inactivation resulted from the myo-inositol deficiency. A previous study in *Slc5a3*-knockout mice has shown that myo-inositol provided at supraphysiologic concentrations can bypass SLC5A3 to enter the cells, possibly via other low-affinity transporters (23). Standard culture medium contains around 0.3 mmol/L myo-inositol, similar to the level detected in human serum (24). Strikingly, with the addition of supplementary myo-inositol in the culture medium, the proliferation of *SLC5A3*-knockout cells was completely rescued (Fig. 3A). Of note, extra myo-inositol did not promote the growth of parental AML cells (Supplementary Fig. S7A). In accordance, depletion of the basal myo-inositol from the culture medium largely impeded the growth of parental AML cells, causing similar phenotypes as *SLC5A3* deletion, with cell context–dependent alterations of cell cycle and induction of apoptotic cell death (Fig. 3B; Supplementary Fig. S7B and S7C). Together, these data reveal that myo-inositol is a critical metabolite for AML.

Because a subset of AML cell lines was not dependent on *SLC5A3* based on the DepMap dataset (Supplementary Fig. S5C), we explored the potential biomarkers associated with *SLC5A3* essentiality in AML. *SLC5A3* was ubiquitously expressed in AML cell lines, and its expression was not correlated with its dependency. Intriguingly, however, the low expression of *inositol-3-phosphate synthase 1* (*ISYNA1*) predicted a strong *SLC5A3* dependency in AML cell lines (Fig. 3C). In addition to importing myo-inositol from the extracellular fluid, cells can also synthesize myo-inositol *de novo* from glucose 6-phosphate, and *ISYNA1* encodes the rate-limiting enzyme in this myo-inositol biosynthesis pathway (25). Thus, we postulated that SLC5A3 becomes essential in AML cells with insufficient myo-inositol biosynthesis capacity. We confirmed the low expression of the ISYNA1 protein in AML cells sensitive to *SLC5A3* deletion, and importantly, overexpression of *ISYNA1* can completely relieve the SLC5A3 dependency (Fig. 3D–F). Moreover, knockout of *ISYNA1* in the ISYNA1-high cell line M07e exacerbated the growth defect associated with *SLC5A3* depletion (Fig. 3G and H). Altogether, these results strongly demonstrate that *SLC5A3* is required for maintaining sufficient myo-inositol levels to support AML proliferation.

MARCH5 Loss Represses AML Cell Growth *In Vitro* and *In Vivo*

We next sought to validate the dependency of AML cells on *MARCH5*. Inactivating MARCH5 via either doxycycline-inducible CRISPR or shRNA systems induced a severe growth defect in various AML cell lines and PDX models (Fig. 4A and B; Supplementary Fig. S8A and S8B). The growth defect could be reversed by a CRISPR-resistant cDNA encoding wild-type *MARCH5*, proving the on-target effect. By contrast, *MARCH5* mutations (H43W and C68S) that disrupt its RING domain and thus ubiquitinase function ablated the rescuing ability (26, 27), indicating the requirement for the catalytic function of MARCH5 in AML (Fig. 4C; Supplementary Fig. S8C and S8D). In addition, for MARCH5 validation, we deployed a dTAG system, which uses a heterobifunctional small molecule that binds the $FKBP12^{F36V}$-fused target protein (i.e., MARCH5) and an E3 ligase complex

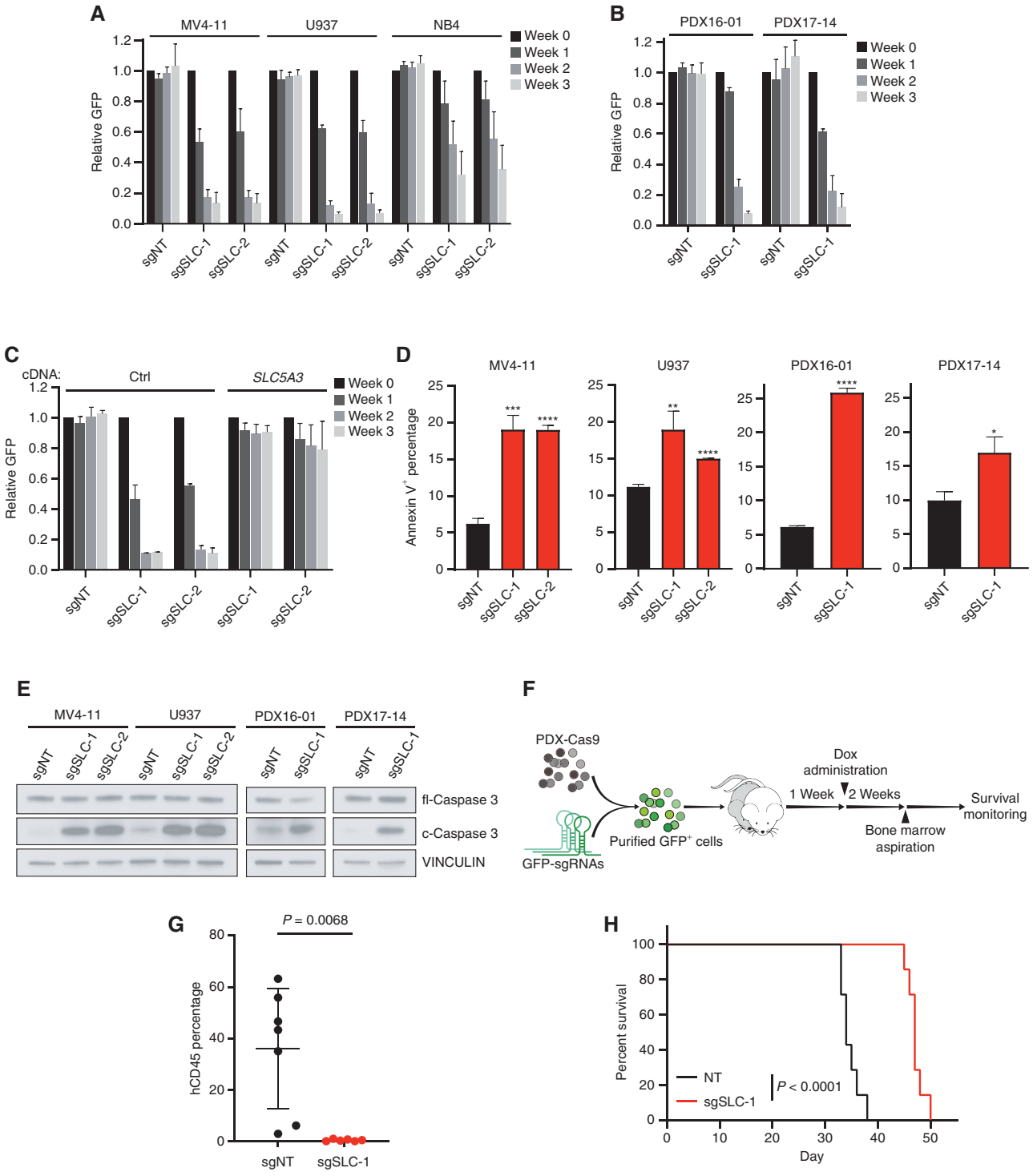

Figure 2. SLC5A3 is essential for AML growth. **A** and **B,** AML cell lines (**A**) and PDX models (**B**) were transduced with nontargeting sgRNA (sgNT) and *SLC5A3* sgRNA (sgSLC-1 and sgSLC-2) vectors that coexpress GFP. Cell growth was evaluated in an *in vitro* competition proliferation assay as measured by the change in percentage of GFP+. **C,** Competitive growth of MV4-11 cells transduced with empty vector (Ctrl) or CRISPR-resistant *SLC5A3* cDNA upon endogenous *SLC5A3* knockout. For **A**–**C**, results represent mean + SD, $n = 2$. **D** and **E,** Flow cytometry analysis of Annexin V (**D**) and immunoblot analysis of full-length (fl) and cleaved (c) caspase 3 (**E**) in AML cells expressing the indicated sgRNAs at day 12 after transduction. For **D**, results represent mean + SD, $n = 3$. *, $P < 0.05$; **, $P < 0.01$; ***, $P < 0.001$; ****, $P < 0.0001$, determined by unpaired two-sided *t* test. **F,** Schematic of evaluating SLC5A3 dependency *in vivo* using PDX cells. NSGS mice were transplanted with PDX16-01 cells expressing doxycycline (Dox)-inducible sgNT or sgSLC-1. Doxycycline-containing food was delivered from day 7 posttransplantation. **G,** Human CD45 flow cytometry analysis to evaluate leukemia burden in bone marrow aspiration samples at 2 weeks after starting doxycycline-containing diet. Mean and SD were plotted; *P* value was calculated by unpaired two-sided *t* test. **H,** Survival curves of mice from **G**. The *P* value was calculated by log-rank test.

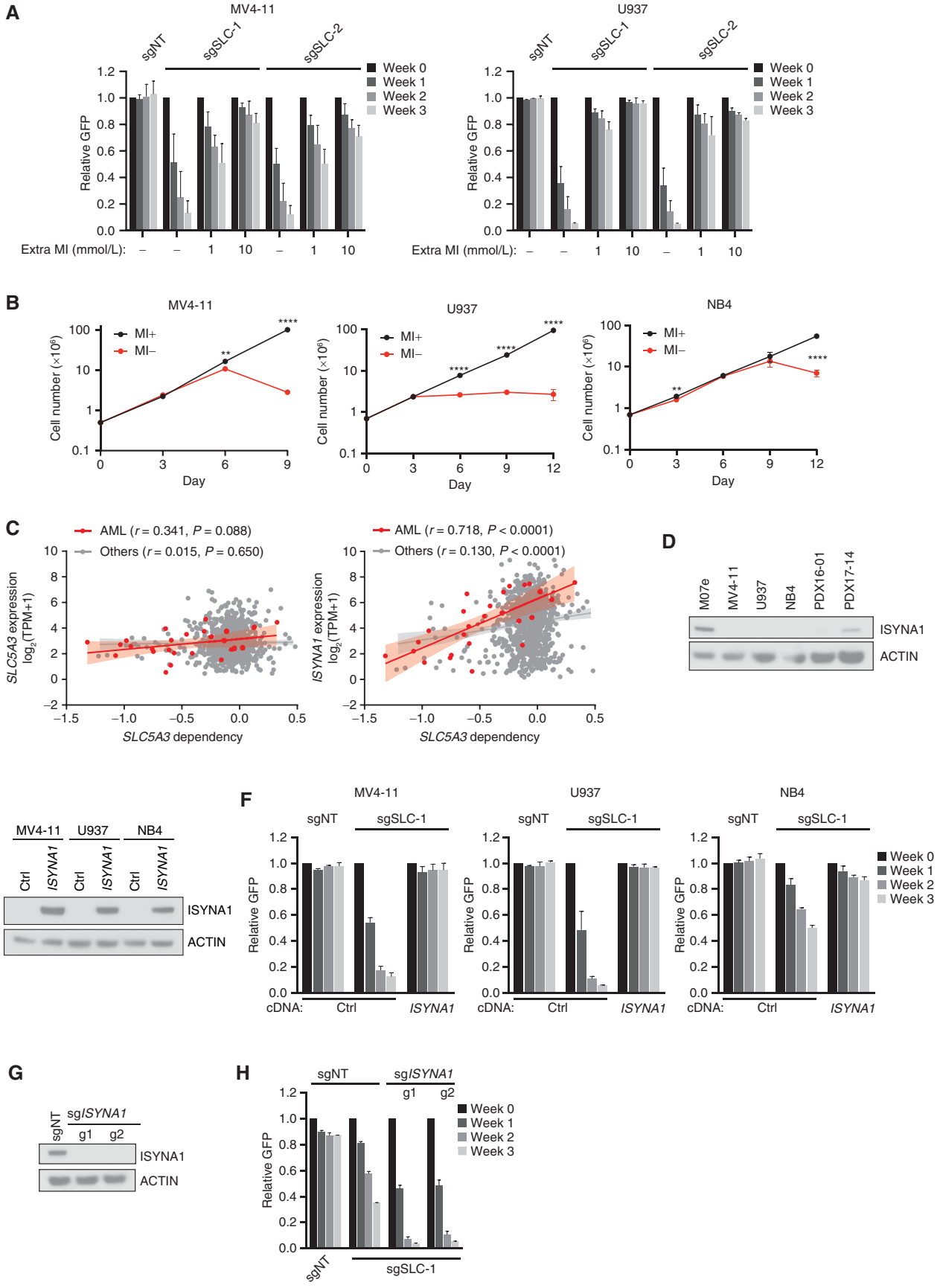
A
MV4-11
U937
sgNT
sgSLC-1
sgSLC-2
Week 0
Week 1
Week 2
Week 3
Relative GFP
Extra MI (mmol/L): – – 1 10 – 1 10
B
MV4-11
U937
NB4
MI+
MI–
Cell number (×10⁶)
Day
C
AML (r = 0.341, P = 0.088)
Others (r = 0.015, P = 0.650)
AML (r = 0.718, P < 0.0001)
Others (r = 0.130, P < 0.0001)
SLC5A3 expression log2(TPM+1)
ISYNA1 expression log2(TPM+1)
SLC5A3 dependency
D
M07e
MV4-11
U937
NB4
PDX16-01
PDX17-14
ISYNA1
ACTIN
E
MV4-11
U937
NB4
Ctrl
ISYNA1
ISYNA1
ACTIN
F
MV4-11
U937
NB4
sgNT
sgSLC-1
Relative GFP
cDNA: Ctrl ISYNA1
G
sgNT
sgISYNA1
g1
g2
ISYNA1
ACTIN
H
sgNT
sgISYNA1
g1
g2
Week 0
Week 1
Week 2
Week 3
Relative GFP
sgNT
sgSLC-1

(i.e., VHL), bringing the two in close proximity and leading to the ubiquitination and proteasome-mediated degradation of the target protein (Supplementary Fig. S8E; ref. 28). We were able to establish the MARCH5 dTAG degradation system in both AML cell line and PDX models in which we deleted endogenous *MARCH5* by CRISPR and expressed exogenous FKBP12^{F36V}-hemagglutinin (HA)–tagged MARCH5 protein at a physiologic level comparable to the endogenous one (Supplementary Fig. S8F). dTAG-MARCH5 cells displayed a similar basal proliferation rate and apoptosis compared with control cells expressing Cas9 only (Supplementary Fig. S8F–S8H). Similar to CRISPR deletion of *MARCH5*, MARCH5 degradation with the dTAG molecule dTAG^{V}-1 markedly impaired cell growth (Fig. 4D and E).

MARCH5 dependency was further confirmed using an *in vivo* competition assay in a third PDX model (PDX68555 with an MLL–AF9 fusion and a *FLT3* mutation). PDX cells expressing a GFP-linked *MARCH5* sgRNA were depleted in NSGS mice, as evidenced by a dramatic reduction of the GFP$^+$ fraction in engrafted cells. In contrast, the PDX cells expressing a nontargeting sgRNA were maintained (Fig. 4F–H). To confirm that the *in vivo* growth disadvantage of *MARCH5*-depleted cells is not caused by homing defects, we used MV4-11 cells expressing luciferase and doxycycline-inducible CRISPR directed against *MARCH5*. Doxycycline-mediated deletion of *MARCH5* posttransplantation led to a marked attenuation of AML progression in NSGS mice as monitored by bioluminescence imaging, which translated to prolonged survival (Fig. 4I–K). We examined the *MARCH5* sgRNA-expressing cells collected from the leukemic mice and found that the *MARCH5* expression was partially restored as compared with the cells with *MARCH5* knockout induced *in vitro*, supporting that loss of MARCH5 is incompatible with AML maintenance (Supplementary Fig. S8I). Collectively, these results demonstrate that targeting MARCH5 can suppress the progression of AML cells both *in vitro* and *in vivo*.

Differential MARCH5 Dependency in Healthy Human Hematopoietic Stem and Progenitor Cells Compared with AML Blasts

We next attempted to determine whether MARCH5 is required by healthy human CD34$^+$ hematopoietic stem and progenitor cells (HSPC). Because of the low efficiency of lentiviral transduction of Cas9 into CD34$^+$ HSPCs, we used the nucleofection of Cas9–sgRNA ribonucleoprotein complexes (RNP) to enable genome editing in these cells and evaluated their progenitor activity via colony formation assays (Fig. 5A). We first validated this approach using AML cells. RNPs containing *MARCH5* sgRNA were introduced into NB4 and AML PDX cells; RNPs with sgRNA targeting a gene desert region in chromosome 2 (sgCHR2) or the common essential gene *RPA3* were also included as negative and positive controls, respectively. A high genome editing efficiency was achieved for all RNPs (Supplementary Fig. S9A). As expected, *MARCH5* deletion dramatically impaired the colony-forming capacity of AML cells, causing a more than 80% reduction of colony number and largely decreasing colony size (Fig. 5B; Supplementary Fig. S9B). We then evaluated CD34$^+$ HSPCs derived from either bone marrow or umbilical cord blood and obtained comparable genome editing efficiency (Supplementary Fig. S9C). In contrast to AML cells, sg*MARCH5*-nucleofected CD34$^+$ cells displayed only a 10% to 30% and 30% to 50% reduction of colony number in the erythroid and myeloid lineages, respectively (Fig. 5C). Colonies of the myeloid lineage were relatively more affected, with a more frequent appearance of smaller and/or less compacted colonies (Supplementary Fig. S9D). Nonetheless, these results highlight that healthy human HSPCs are less dependent on MARCH5 compared with AML cells, supporting the potential therapeutic window for MARCH5-targeted treatment.

MARCH5 Prevents Apoptosis in AML

MARCH5 inactivation in AML cells resulted in a slight reduction of S phase and increase in sub-G1 and G1/G0 phases (Supplementary Fig. S10A and S10B). Induction of the sub-G1 phase suggested the occurrence of cell death. Indeed, apoptosis was consistently observed and strongly induced in some models, as indicated by upregulated cleaved caspase 3 and Annexin V (Fig. 6A and B; Supplementary Fig. S10C). In PDX17-14, which was highly sensitive to MARCH5 inhibition, 2-hour treatment with dTAG^{V}-1 was sufficient to prime cells for apoptosis, as indicated by BH3 profiling (Supplementary Fig. S10D; ref. 29). Importantly, knockout of the mitochondrial apoptosis effectors *BAX* or *BAK1* reversed the apoptosis induction and growth defect of *MARCH5*-null cells (Fig. 6C; Supplementary Fig. S10E–S10G). AML cell lines displayed differential reliance on *BAX* and *BAK1* for the execution of MARCH5 depletion–mediated apoptosis, and in some models, such as NB4 and PDX17-14, double knockout of *BAX* and *BAK1* was required to rescue MARCH5 inactivation (Fig. 6D; Supplementary Fig. S10H and S10I). These findings demonstrate that apoptosis induction is an essential cellular mechanism accounting for the inhibitory effect of MARCH5 depletion in AML.

The activation of the mitochondrial apoptotic pathway is determined by the counterbalance between proapoptotic and antiapoptotic BCL2 family proteins (30). Strikingly, multiple genome-wide screens revealed that the dependency scores of *MARCH5* and *MCL1*, but not other antiapoptotic BCL2

Figure 3. Myo-inositol imported via SLC5A3 sustains AML. **A,** Competitive growth was evaluated for *SLC5A3*-knockout MV4-11 and U937 cells in regular culture medium, which contains ~0.3 mmol/L myo-inositol (MI), or culture medium supplemented with extra MI at the indicated concentrations. sgNT, nontargeting sgRNA; sgSLC-1 and sgSLC-2, *SLC5A3* sgRNA vectors. **B,** Cumulative cell growth of AML cells in myo-inositol–depleted medium with (MI+) or without (MI−) 0.3 mmol/L myo-inositol reconstituted. Results represent mean ± SD, $n = 3$. **, $P < 0.01$; ****, $P < 0.0001$, determined by unpaired two-sided t test. **C,** Scatter plots showing the linear correlation between CERES dependency scores of *SLC5A3* and the expression level of *SLC5A3* or *ISYNA1* across AML cell lines ($n = 26$) or other cancer cell lines ($n = 904$) in the DepMap dataset. Each dot represents a cell line; the shaded area represents the 95% confidence level interval for the linear model. TPM, transcripts per kilobase million. **D,** Immunoblot analysis of ISYNA1 protein levels in AML cells. The M07e cell line was used as a control with high ISYNA1 expression. **E,** Immunoblot confirming the overexpression of *ISYNA1* in the indicated AML cells. **F,** Competitive growth of AML cells with or without *ISYNA1* overexpression upon *SLC5A3* knockout. **G,** Immunoblot analysis of ISYNA1 in M07e cells transduced with sgNT or *ISYNA1* sgRNAs. **H,** Competitive growth of cells in **G** was evaluated upon *SLC5A3* deletion. For **A**, **F**, and **H**, results represent mean + SD, $n = 2$.

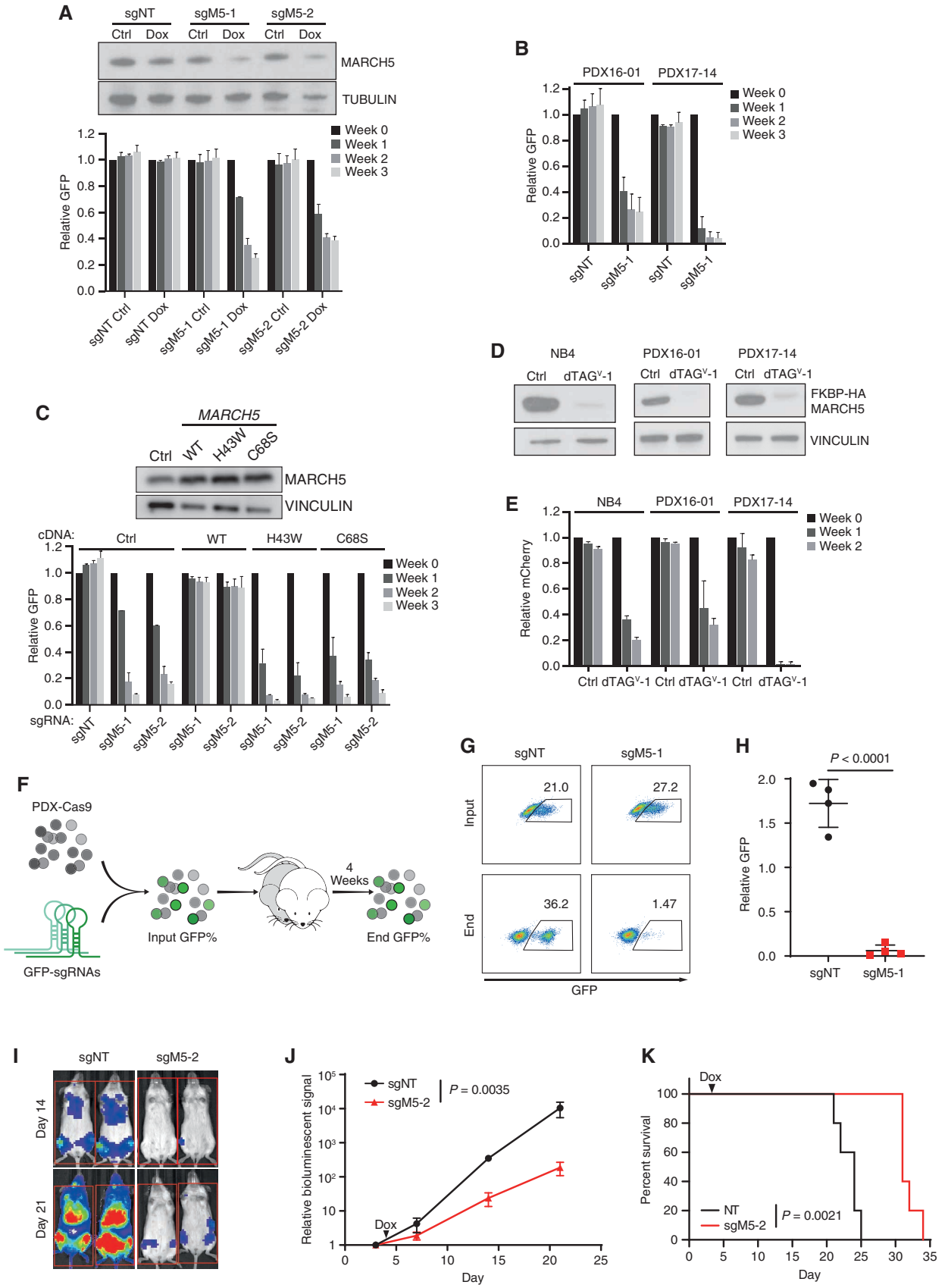
A
sgNT
sgM5-1
sgM5-2
Ctrl Dox Ctrl Dox Ctrl Dox
MARCH5
TUBULIN
Relative GFP
Week 0
Week 1
Week 2
Week 3
sgNT Ctrl
sgNT Dox
sgM5-1 Ctrl
sgM5-1 Dox
sgM5-2 Ctrl
sgM5-2 Dox
B
PDX16-01
PDX17-14
Relative GFP
Week 0
Week 1
Week 2
Week 3
sgNT
sgM5-1
sgNT
sgM5-1
C
MARCH5
Ctrl WT H43W C68S
MARCH5
VINCULIN
cDNA:
Ctrl
WT
H43W
C68S
Relative GFP
Week 0
Week 1
Week 2
Week 3
sgRNA:
sgNT
sgM5-1
sgM5-2
sgM5-1
sgM5-2
sgM5-1
sgM5-2
sgM5-1
sgM5-2
D
NB4
PDX16-01
PDX17-14
Ctrl dTAGV-1 Ctrl dTAGV-1 Ctrl dTAGV-1
FKBP-HA
MARCH5
VINCULIN
E
NB4
PDX16-01
PDX17-14
Relative mCherry
Week 0
Week 1
Week 2
Ctrl dTAGV-1 Ctrl dTAGV-1 Ctrl dTAGV-1
F
PDX-Cas9
GFP-sgRNAs
Input GFP%
4 Weeks
End GFP%
G
sgNT
sgM5-1
Input
End
21.0
27.2
36.2
1.47
GFP
H
P < 0.0001
Relative GFP
sgNT
sgM5-1
I
sgNT
sgM5-2
Day 14
Day 21
J
sgNT
sgM5-2
P = 0.0035
Relative bioluminescent signal
Dox
Day
K
Dox
Percent survival
NT
sgM5-2
P = 0.0021
Day

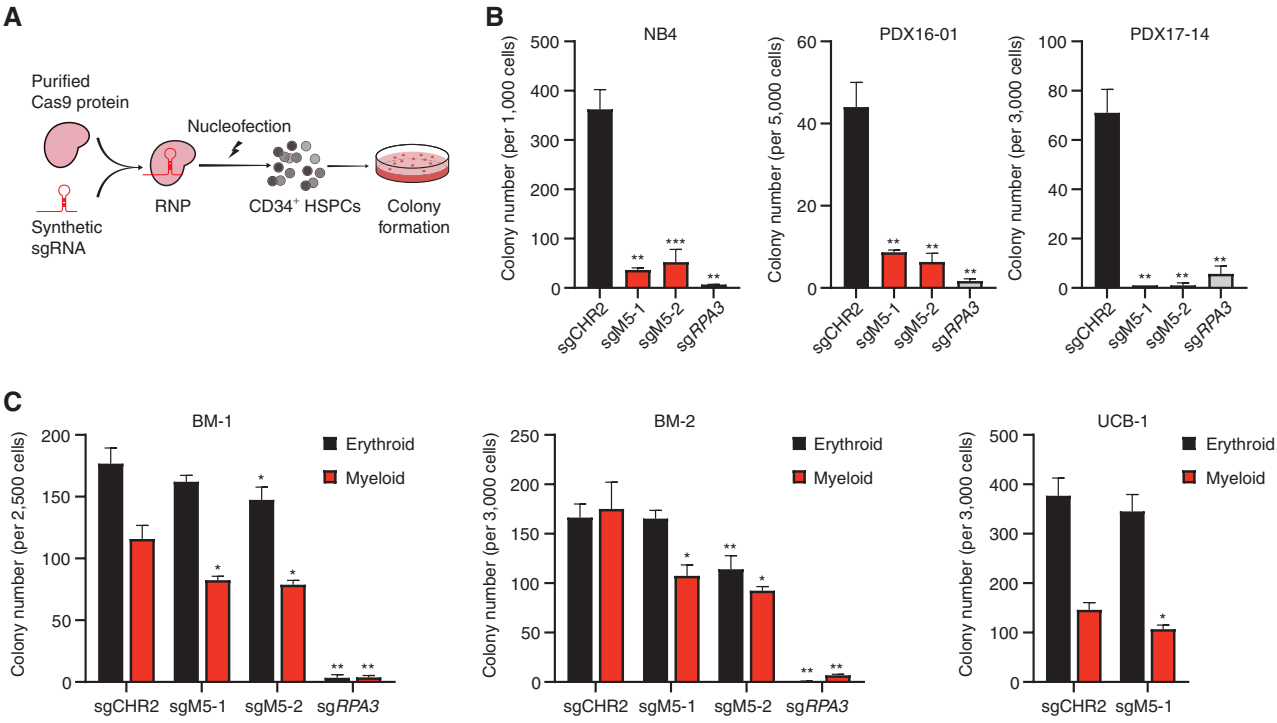

Figure 5. Human CD34+ HSPCs are less dependent on MARCH5 for colony formation compared with AML cells. **A,** Schematic of evaluating the essentiality of MARCH5 in colony formation of human HSPCs via nucleofection. **B** and **C,** Colony formation assays of AML cells (**B**) or CD34+ HSPCs (**C**) nucleofected with the indicated RNPs. CD34+ cells were derived from bone marrow (BM) or umbilical cord blood (UCB) from three independent donors. Results represent mean + SD, $n = 3$. *, $P < 0.05$; **, $P < 0.01$; ***, $P < 0.001$, determined by unpaired two-sided *t* test. sgM5-1 and sgM5-2, *MARCH5* sgRNA RNPs.

family genes, were significantly correlated across the AML cell lines as well as other cancer models (Fig. 6E and F; Supplementary Fig. S11A), suggesting a functional connection between *MARCH5* and *MCL1*. This compelled us to test whether overexpression of antiapoptotic BCL2 family proteins can reverse the effect of MARCH5 inhibition. Overexpression of *MCL1* did not robustly rescue *MARCH5* deletion, particularly in the models most sensitive to loss of MARCH5, but overexpression of *BCL2* or *BCLXL* invariably rescued the growth impairment caused by MARCH5 depletion in AML (Fig. 6G and H; Supplementary Fig. S11B). This inconsistent rescuing ability of overexpressed MCL1 is in accordance with altered MCL1 function upon loss of MARCH5.

We then investigated whether MARCH5 depletion can modulate the expression of BCL2 family members. Although most BCL2 proteins remained unaltered, an upregulation of MCL1 and NOXA, a BH3-only proapoptotic protein known to interact with and inhibit MCL1, was observed, which is consistent with the previous findings that MARCH5 was responsible for degrading the MCL1–NOXA complex (Fig. 6I; Supplementary Fig. S10G; refs. 31, 32). Although total levels of MCL1 increased, its localization primarily to the mitochondria did not change (Supplementary Fig. S11C). Recent studies suggest that increased NOXA mediates several downstream events of MARCH5 inhibition, such as sensitizing cells to stress stimuli (32–34). To investigate whether increased NOXA levels also account for the apoptosis induction in AML cells, *NOXA*-knockout cells were generated. Strikingly, MARCH5 depletion caused defective growth and induced cell death in *NOXA*-null cells to the same degree as

Figure 4. MARCH5 inhibition suppresses AML cell growth. **A,** MV4-11 cells were transduced with doxycycline (Dox)-inducible nontargeting sgRNA (sgNT) and *MARCH5* sgRNA (sgM5-1 and sgM5-2) vectors that coexpress GFP. Immunoblot analysis of MARCH5 was performed on day 6 after doxycycline treatment (top). Cell growth was evaluated in a competition proliferation assay (bottom). **B,** Competitive growth of Cas9-PDX cells transduced with GFP-linked sgNT or sgM5-1. **C,** Immunoblot analysis of MV4-11 cells expressing an empty vector (Ctrl), CRISPR-resistant *MARCH5* wild-type (WT), or ligase-defective mutant (H43W or C68S) cDNA (top). Competitive growth of these cells was evaluated upon endogenous *MARCH5* knockout (bottom). **D,** Immunoblot analysis of FKBP-HA-MARCH5 with HA antibody in dTAG-MARCH5 AML cells treated with 500 nmol/L dTAG^V-1 for 24 hours (NB4), 4 hours (PDX16-01), or 2 hours (PDX17-14). **E,** Competitive growth of dTAG-MARCH5 AML cells treated with DMSO (Ctrl) or 500 nmol/L dTAG^V-1. For **A**–**C** and **E**, results represent mean + SD, $n = 2$. **F,** Schematic of *in vivo* competition assay with PDX cells. Mouse bone marrow cells were collected for evaluating end GFP+ percentage. **G,** Representative flow cytometry analysis of input and end GFP percentage of sgNT- or sgM5-1–expressing cells. **H,** Relative abundance of PDX cells expressing sgNT or sgM5-1, as calculated by normalizing end GFP percentage to input GFP percentage. The *P* value was calculated by unpaired two-tailed *t* test, $n = 4$. **I,** NSGS mice were transplanted with MV4-11 cells expressing doxycycline-inducible sgNT or sgM5-2. Doxycycline-containing food was served from day 4 posttransplantation. Representative bioluminescence images are shown on the indicated day posttransplantation. **J,** Quantification of serial bioluminescence imaging. The data were normalized to the baseline readout on day 3. $n = 5$; results represent mean ± SD. The *P* value was calculated using unpaired two-tailed *t* test with measurements on day 21. **K,** Survival curves of mice used in **J**. The *P* value was calculated by log-rank test.

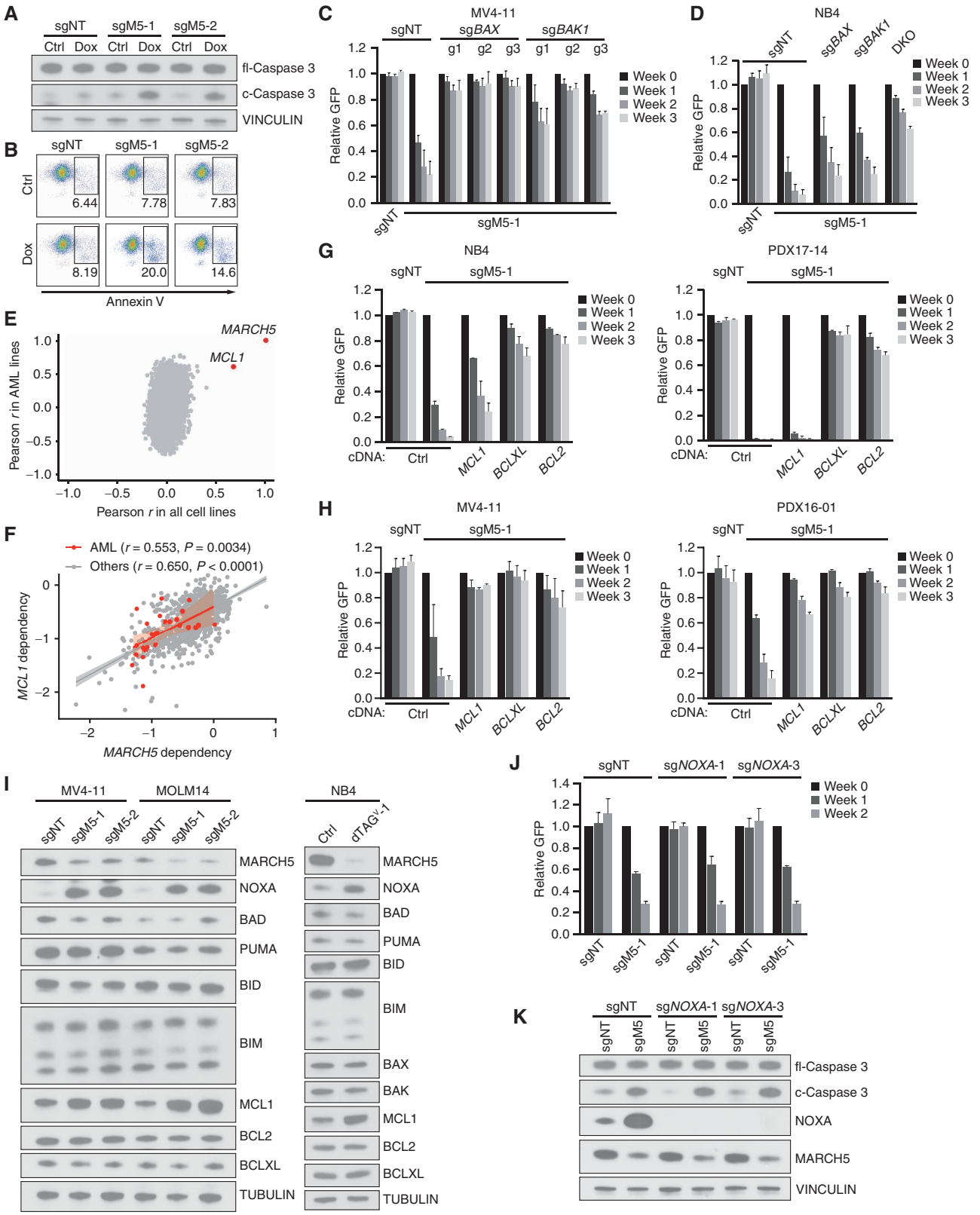
A
sgNT
sgM5-1
sgM5-2
Ctrl Dox Ctrl Dox Ctrl Dox
fl-Caspase 3
c-Caspase 3
VINCULIN
B
sgNT
sgM5-1
sgM5-2
Ctrl
Dox
6.44
7.78
7.83
8.19
20.0
14.6
Annexin V
C
MV4-11
sgNT
sgBAX
sgBAK1
g1 g2 g3 g1 g2 g3
Relative GFP
Week 0
Week 1
Week 2
Week 3
sgNT
sgM5-1
D
NB4
sgNT
sgBAX
sgBAK1
DKO
Relative GFP
Week 0
Week 1
Week 2
Week 3
sgNT
sgM5-1
E
MARCH5
MCL1
Pearson r in AML lines
Pearson r in all cell lines
F
AML (r = 0.553, P = 0.0034)
Others (r = 0.650, P < 0.0001)
MCL1 dependency
MARCH5 dependency
G
NB4
sgNT
sgM5-1
Relative GFP
Week 0
Week 1
Week 2
Week 3
cDNA:
Ctrl
MCL1
BCLXL
BCL2
PDX17-14
sgNT
sgM5-1
Relative GFP
Week 0
Week 1
Week 2
Week 3
cDNA:
Ctrl
MCL1
BCLXL
BCL2
H
MV4-11
sgNT
sgM5-1
Relative GFP
Week 0
Week 1
Week 2
Week 3
cDNA:
Ctrl
MCL1
BCLXL
BCL2
PDX16-01
sgNT
sgM5-1
Relative GFP
Week 0
Week 1
Week 2
Week 3
cDNA:
Ctrl
MCL1
BCLXL
BCL2
I
MV4-11
MOLM14
sgNT
sgM5-1
sgM5-2
sgNT
sgM5-1
sgM5-2
MARCH5
NOXA
BAD
PUMA
BID
BIM
MCL1
BCL2
BCLXL
TUBULIN
NB4
Ctrl
dTAG V-1
MARCH5
NOXA
BAD
PUMA
BID
BIM
BAX
BAK
MCL1
BCL2
BCLXL
TUBULIN
J
sgNT
sgNOXA-1
sgNOXA-3
Relative GFP
Week 0
Week 1
Week 2
sgNT
sgM5-1
sgNT
sgM5-1
sgNT
sgM5-1
K
sgNT
sgNOXA-1
sgNOXA-3
sgNT
sgM5
sgNT
sgM5
sgNT
sgM5
fl-Caspase 3
c-Caspase 3
NOXA
MARCH5
VINCULIN

in control cells (Fig. 6J and K). Given the possible redundant roles among BH3 protein members, we also examined *BIM*-knockout cells, as well as *BIM*/*NOXA* double-knockout cells. However, neither of these displayed improved resistance to MARCH5 inhibition compared with control cells (Supplementary Fig. S11D and S11E). In fact, knockout of *BID* or *BIK*, two other BH3 members capable of neutralizing MCL1, was not able to rescue *MARCH5* knockout (Supplementary Fig. S11F and S11G). Together, these results show that the diminished MCL1 antiapoptotic activity upon MARCH5 depletion is not caused by a loss of MCL1 expression or by enhanced activity of other proapoptotic BCL2 members but rather likely the alteration of other downstream mediators of MARCH5.

MARCH5 Depletion Sensitizes AML Cells to Venetoclax

Apoptosis sensitivity can determine the response to various therapies in cancer (29). Because loss of MARCH5 primed AML cells for apoptosis, we investigated whether MARCH5 inhibition can sensitize AML cells to anticancer therapies. Control and *MARCH5*-knockdown OCI-AML2 cells were subjected to a chemical screen across a library of 3,247 anticancer compounds. Fifty-eight compounds displayed an enhanced inhibitory effect on *MARCH5*-knockdown cells compared with control cells. Notably, the BH3 mimetics, a class of small molecules that mimic BH3 proteins to bind and inhibit antiapoptotic BCL2 proteins, were enriched (Fig. 7A–C; Supplementary Fig. S12A). These data prompted us to examine whether MARCH5 inactivation in AML cells enhances their sensitivity to venetoclax, a BH3 mimetic that specifically blocks BCL2 and is FDA approved for the treatment of older adults with AML in combination with a hypomethylating agent (35). *MARCH5* deletion through inducible CRISPR indeed sensitized AML cells to venetoclax (Fig. 7D). Similarly, dTAG^V-1 treatment elicited a dramatic venetoclax sensitizing effect in dTAG-MARCH5 cells but not in control cells (Fig. 7E; Supplementary Fig. S12B). Upregulation of MCL1 or BCLXL activity has been identified as a mechanism causing venetoclax resistance (36). Consistent with the loss of MARCH5 impairing MCL1 function, while MARCH5 depletion did not alleviate venetoclax resistance caused by *BCLXL* overexpression, it can diminish MCL1-induced venetoclax resistance (Fig. 7F and G; Supplementary Fig. S12C), even in the AML models whose growth impairment with *MARCH5* knockout is rescued by MCL1 (Fig. 6H; MV4-11 and PDX16-01), highlighting a synergistic cooperation between MARCH5 ablation and venetoclax. NOXA levels are another determinant of venetoclax response consistent with its antagonistic function on MCL1 (37). Accordingly, MARCH5 inhibition also attenuated the venetoclax resistance resulting from *NOXA* knockout (Supplementary Fig. S12D). Overall, the results further support the notion that MARCH5 can regulate MCL1 function through a NOXA-independent manner in AML cells.

The cooperativity between MARCH5 inhibition and venetoclax was also demonstrated *in vivo* using the xenograft model of luciferase-expressing MV4-11 cells. We used a venetoclax dose that is below the maximum tolerated dose in mice, and although this venetoclax regimen showed minimal efficacy in control cells, it enhanced the antileukemic activity of MARCH5 depletion *in vivo* (Fig. 7H and I). There are currently no small-molecule inhibitors directed against MARCH5. We thus deployed the dTAG system as an approximation of pharmacologic inhibition of MARCH5 and investigated its impact in combination with venetoclax in an orthotopic PDX model of AML. To this end, we first characterized the dose and schedule of dTAG^V-1 to achieve maximum *in vivo* degradation. NSGS mice injected with PDX17-14 dTAG-MARCH5 cells were treated with a series of doses of dTAG^V-1 via intravenous administration once daily or intraperitoneal administration twice daily for 4 days, and then FKBP-HA-MARCH5 levels were evaluated by intracellular staining with antibodies against HA-tag (Fig. 7J). Concordant results were obtained with two independent HA antibodies, showing that dTAG^V-1 treatment led to dose-dependent MARCH5 degradation *in vivo*. Maximal achievable degradation was observed at 40 mg/kg—the highest dose that can be achieved given the solubility limitation of the compound (Supplementary Fig. S12E and S12F). Intraperitoneal administration twice daily at 40 mg/kg resulted in similar degradation efficacy compared with intravenous administration once daily (Supplementary Fig. S12G). The intraperitoneal regimen was subsequently chosen for efficacy studies given its improved tolerability to daily intravenous administrations. An independent cohort of mice receiving PDX17-14 dTAG-MARCH5 cells was assigned to four groups and treated with vehicle, venetoclax, dTAG^V-1, or both venetoclax and dTAG^V-1. The leukemic burden in bone marrow was evaluated after 2 weeks of treatment (Fig. 7J). Venetoclax did not elicit a clear antileukemic effect. Although dTAG^V-1 induced a modest reduction in leukemic burden, the combination treatment markedly decreased leukemic burden (Fig. 7K). All told, these results highlight the combinational targeting of MARCH5 and BCL2 as a potential therapeutic approach for AML.

Figure 6. Inhibition of MARCH5 activates the mitochondrial apoptosis pathway. **A** and **B,** Immunoblot analysis of full-length (fl) and cleaved (c) caspase 3 (**A**) and flow cytometry analysis of Annexin V (**B**) in MV4-11 cells transduced with the indicated sgRNAs at day 10 after doxycycline (Dox) treatment. sgNT, nontargeting sgRNA; sgM5-1 and sgM5-2, *MARCH5* sgRNA vectors. **C,** Competitive growth was evaluated for the control or *BAX*/*BAK1*-knockout MV4-11 cells, which were generated with three independent sgRNAs each, upon *MARCH5* deletion. **D,** Competitive growth assay for control, *BAX*-, *BAK1*-, and double (DKO)–knockout NB4 cells with *MARCH5* depletion. **E,** Scatter plot showing the Pearson correlations between CERES dependency scores of *MARCH5* and each other gene across AML cell lines or all cancer cell lines in the DepMap CRISPR screen dataset. Each dot represents a gene. **F,** Scatter plot showing the linear correlation between CERES dependency scores of *MARCH5* and *MCL1* across AML cell lines or other cancer cell lines in the DepMap dataset. Each dot represents a cell line; the shaded area represents the 95% confidence level interval for the linear model. **G** and **H,** Competitive growth of AML cells expressing a control vector or antiapoptotic BCL2 proteins with *MARCH5* knockout. MCL1 displayed distinct rescue effects in cell lines in **G** compared with **H**. **I,** Immunoblot analysis of BCL2 family proteins in AML cells with MARCH5 depletion via sgRNA or dTAG^V-1. **J,** Competition proliferation assays to evaluate the growth effect of MARCH5 depletion in control and *NOXA*-knockout MV4-11 cells. **K,** Immunoblot analysis of full-length and cleaved caspase 3 in control and *NOXA*-knockout MV4-11 cells with MARCH5 deletion. For **C**, **D**, **G**, **H**, and **J**, results represent mean + SD, $n = 2$.

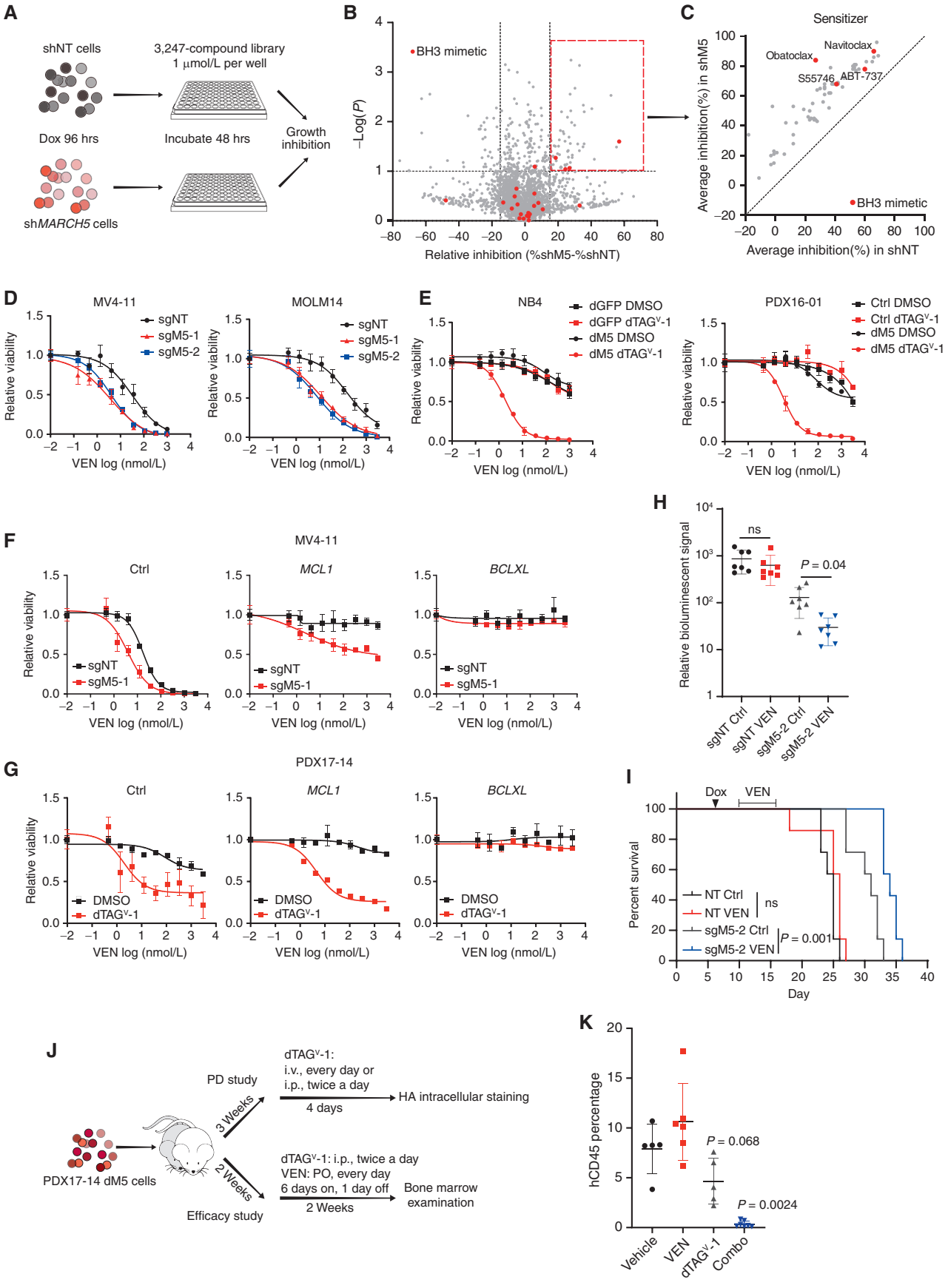
A
shNT cells
3,247-compound library
1 μmol/L per well
Dox 96 hrs
Incubate 48 hrs
Growth inhibition
shMARCH5 cells
B
BH3 mimetic
−Log(P)
Relative inhibition (%shM5-%shNT)
C
Sensitizer
Obatoclax
Navitoclax
S55746
ABT-737
BH3 mimetic
Average inhibition(%) in shM5
Average inhibition(%) in shNT
D
MV4-11
MOLM14
sgNT
sgM5-1
sgM5-2
Relative viability
VEN log (nmol/L)
E
NB4
dGFP DMSO
dGFP dTAGV-1
dM5 DMSO
dM5 dTAGV-1
PDX16-01
Ctrl DMSO
Ctrl dTAGV-1
dM5 DMSO
dM5 dTAGV-1
F
MV4-11
Ctrl
MCL1
BCLXL
G
PDX17-14
DMSO
dTAGV-1
H
Relative bioluminescent signal
ns
P = 0.04
sgNT Ctrl
sgNT VEN
sgM5-2 Ctrl
sgM5-2 VEN
I
Dox
VEN
Percent survival
NT Ctrl
NT VEN
sgM5-2 Ctrl
sgM5-2 VEN
ns
P = 0.001
Day
J
PDX17-14 dM5 cells
PD study
3 Weeks
dTAGV-1:
i.v., every day or
i.p., twice a day
4 days
HA intracellular staining
Efficacy study
2 Weeks
dTAGV-1: i.p., twice a day
VEN: PO, every day
6 days on, 1 day off
2 Weeks
Bone marrow examination
K
hCD45 percentage
P = 0.068
P = 0.0024
Vehicle
VEN
dTAGV-1
Combo

DISCUSSION

Large-scale genome-wide CRISPR screening has provided numerous candidate AML targets, yet uncertainty remains about their physiologic relevance and translational potential. *In vivo* CRISPR screens offer a strategy for identifying leukemia dependencies within the context of the physiologic microenvironment. Our study thus aimed to refine the candidate list by providing *in vivo* functional references to better inform future studies. We have developed an *in vivo* CRISPR screening pipeline in orthotopic xenograft models of human AML and defined experimental conditions necessary for an optimal *in vivo* screen. One major consideration is the requirement for sufficient *in vivo* library representation to avoid false-positive hits. Because AML is established by leukemia-initiating cells, only a subset of the AML cell population retains this leukemia-initiating activity in mouse recipients. As evidenced by our barcoding experiments, random sets of barcodes prevailed in different individual recipients, reflecting the selective leukemia-initiating activity and clonal expansion. Therefore, it is critical to use irradiation to maximize the engraftment capacity of AML cells and include multiple mice to achieve complete *in vivo* library representation. The number of mouse recipients must be adjusted according to the library size and the leukemia-initiating capacity of the model.

PDXs provide useful preclinical models for therapy evaluation. These models largely retain the histologic and genetic characteristics of the primary disease and have also been shown to be predictive of clinical outcome (9). Although PDX models have been widely used for drug evaluation, we established CRISPR-competent PDX models to determine whether the dependency landscape obtained from the cell lines is reflected in PDXs. Quite strikingly, dependencies identified across AML cell line models were strongly recapitulated in the PDX model that we evaluated. We also observed a strong correlation between the *in vitro* and *in vivo* dependencies, likely related to the reduced off-target effects of CRISPR compared with other approaches, such as RNAi, and the robust library representation. However, a few genes reproducibly appeared as *in vitro*–only dependencies, demonstrating that the microenvironment can influence the essentiality of a target. Although our current study was not positioned to discover *in vivo*–specific dependencies, our pipeline is adaptable for *de novo* dependency discovery in human AML when coupled with other focused libraries. In general, PDX models with reproducible engrafting capacity and relatively short disease latency are preferred for *in vivo* CRISPR screening. Reports from other groups and our own experience indicate that AML PDX models can be more readily established from disease subtypes with intermediate and poor prognosis (38). Although PDX models with MLL fusions and a CALM–AF10 fusion were used in this study, it should be feasible to establish CRISPR-competent PDX models with different genetic backgrounds and thus extend our dependency discovery capacity to other high-risk subtypes of AML.

Metabolic reprogramming contributes to tumor development and sustains cancer cell proliferation. Like other cancers, AML has altered metabolic features and is addicted to certain metabolites and metabolic pathways for survival, providing new possibilities for AML treatment. For instance, the one-carbon folate pathway is reported to be critical for AML growth, and AML stem cells selectively depend on amino acid metabolism to fuel oxidative phosphorylation. Accordingly, blocking these pathways has exhibited antileukemic activity in preclinical studies (39, 40). Here, we revealed myo-inositol as a metabolic dependency in AML. Our data suggest that AML cells rely on either SLC5A3-mediated extracellular transportation or ISYNA1-mediated intracellular *de novo* synthesis for their myo-inositol supply, and AML cells with low ISYNA1 levels depend on SLC5A3 exclusively for fueling myo-inositol metabolism. Interestingly, the SLC5A3–ISYNA1 correlation is less evident in other cancer types; most ISYNA1 low–expressing cancer cell lines are not dependent on SLC5A3. The underlying biology rendering SLC5A3 as a selective dependency in ISYNA1-low AML but not in other ISYNA1-low cancers is not clear. It is possible that the myo-inositol addiction is endowed by the cell lineage in AML or that alternative myo-inositol transporters are used in ISYNA1 low–expressing cancer cells that are not SLC5A3 dependent. Although SLC5A3-specific inhibitors have not been reported, small-molecule inhibitors against SLC5A1 and SLC5A2—two solute carrier family 5 members with a similar structure to SLC5A3—have been developed (41, 42). Therefore, SLC5A3 is potentially actionable, and our study supports the development of chemical probes against this strong AML dependency.

Mitochondrial physiology constitutes another important axis in AML disease maintenance and drug response. It is

Figure 7. Inactivating MARCH5 enhances the antileukemic activity of venetoclax. **A,** Schematic of chemical screen; 1 μmol/L of each compound was used in the screen. Dox, doxycycline. **B** and **C,** Scatter plots showing the relative inhibitory effect of screening chemical compounds in *MARCH5*-knockdown cells (shM5) compared with control cells (shNT; **B**). Each dot represents a compound. The relative inhibition is the mean difference of percentage of growth inhibition between shM5 and shNT cells. *P* values were calculated by unpaired two-tailed *t* test, $n = 2$. A cutoff of $P \leq 0.1$ and relative inhibition ≥15% were used to select compounds displaying the enhanced inhibitory effect on shM5 cells, which were present in **C**. Compounds within the class of BH3 mimetics are noted. **D** and **E,** Relative viability of doxycycline-inducible sgRNA-expressing cells (**D**) or dTAG-MARCH5 (dM5) cells (**E**) treated with venetoclax (VEN) for 3 days. Cells were treated with doxycycline for 4 days prior or 500 nmol/L $dTAG^V$-1 concurrently with venetoclax treatment. Cells expressing FKBP-GFP (dGFP) or Cas9 only (Ctrl) were included as a control for dTAG-MARCH5 cells. sgNT, nontargeting sgRNA; sgM5-1 and sgM5-2, *MARCH5* sgRNA vectors. **F** and **G,** Relative viability of control, *MCL1*-, or *BCLXL*-overexpressing cells with venetoclax treatment upon *MARCH5* knockout (**F**) or degradation (**G**). For **D**–**G**, cell viability was determined by CellTiter-Glo and normalized to the DMSO-treated control. The mean ± SD ($n = 4$) and dose–response curves are plotted. **H,** NSGS mice were transplanted with MV4-11 cells expressing doxycycline-inducible sgNT or *MARCH5* sg-2. Doxycycline-containing food was served from day 7 posttransplantation. Mice were treated for 1 week with 75 mg/kg venetoclax by oral gavage daily starting at day 10 posttransplantation. Quantification of bioluminescence imaging on day 18 is shown. The data were normalized to the baseline readout on day 3. $n = 7$; results represent mean ± SD. The *P* values were calculated using unpaired two-tailed *t* test. ns, not significant. **I,** Survival curves of mice used in **H**. The *P* values were calculated by log-rank test. **J,** Schematic for characterizing the *in vivo* pharmacodynamics (PD) of $dTAG^V$-1 and evaluating the synergy between MARCH5 degradation and venetoclax *in vivo*. PO, *per os*. **K,** Human CD45 flow cytometry analysis to evaluate leukemia burden in bone marrow after a 2-week treatment. Mean and SD were plotted, and *P* values were calculated by unpaired two-sided *t* test.

therefore particularly relevant that MARCH5, a target located in the outer mitochondrial membrane, scored as a top hit in our screens. MARCH5 has been reported to serve multiple context-dependent functions in cells, including regulation of mitochondrial dynamics through its modulation of fission or fusion effector proteins, such as DRP1 and MFN2 (21); protection against stress stimuli through facilitation of mitochondria homeostasis or regulation of stress-responding proteins such as inositol-requiring kinase 1 and NOXA (27, 32, 33, 43, 44); and prevention of persistent innate immune response through the reduction of mitochondrial antiviral signaling aggregates (45). In contrast, in the case of AML, we have revealed that MARCH5 is essential for cell survival under physiologic conditions; inhibiting MARCH5 by itself is sufficient to activate the canonical mitochondrial apoptosis pathway in a BAX/BAK1-dependent manner. The dependency correlation analysis and our functional studies strongly suggest that MARCH5 regulates apoptosis by interfering with MCL1 function. Although the mechanism by which MARCH5 loss represses MCL1 activity is not fully delineated, we have ruled out several possibilities, including reduction of MCL1 expression, relocation of MCL1 from the mitochondria, or induction of NOXA. Prior studies of a MARCH5–NOXA connection have focused on cellular response to stress inducers where NOXA loss is reported to attenuate the impact of MARCH5 repression. In contrast, our study evaluated the impact of MARCH5 directly in apoptosis regulation. In this latter context, *NOXA* knockout is insufficient to rescue MARCH5 repression. All told, our results are consistent with MARCH5 playing a regulatory role in MCL1 activity, possibly through posttranslational modification or through another mediator of MCL1 function—mechanisms that will be the study of future investigations.

Venetoclax has received FDA approval for the treatment of newly diagnosed older adult patients with AML in combination with hypomethylating agents. This promising combination has resulted in a remission rate of approximately 70%. However, intrinsic and acquired resistance still emerged in a significant percentage of patients, and the efficacy of this combination drops precipitously in patients with relapsed and refractory AML (35). Thus, additional combination approaches are desired to enhance the clinical benefits of venetoclax. Overcoming venetoclax resistance via targeting mitochondrial components is an emerging theme. Blockage of oxidative phosphorylation activity, inhibition of mitochondrial translation, and disruption of mitochondrial cristae structures can all result in venetoclax sensitization in AML cells (40, 46, 47). Consistent with previous reports showing that loss of MARCH5 sensitizes cells to BH3 mimetics (27, 33), our data have demonstrated that MARCH5 is another promising synergistic mitochondrial target for enhancing the efficacy of venetoclax in AML. Given that MARCH5 inhibition can reverse the venetoclax resistance caused by *MCL1* overexpression and *NOXA* deletion, but not that caused by *BCLXL* overexpression, it is likely that the MCL1 repression also contributes to the venetoclax sensitization conferred by MARCH5 depletion. Collectively, MARCH5 is positioned as a strong AML dependency, as well as a synergistic target for anti-BCL2 therapy. With the success of targeting other E3 ligases (e.g., MDM2 and XIAP) by small molecules already in clinical testing in humans (48, 49), and given that the enzymatic activity of MARCH5 is critical, MARCH5 targeting holds promise for patients with AML and potentially the treatment of other malignancies.

Taken together, our *in vivo* screening approach, coupled with CRISPR-competent PDX models, constitutes a platform for prioritizing AML targets emerging from *in vitro* screens for therapy development, with SLC5A3 and MARCH5 nominated as two top targets for further consideration in AML. According to the DepMap dataset, strong *MARCH5* dependency is observed in AML cell lines with various French–American–British (FAB) subtypes and genetic contexts, suggesting broad applicability. By contrast, it is intriguing that strong *SLC5A3* dependency is enriched in AML cell lines of the FAB M5 subtype, which are also enriched for MLL fusions (Supplementary Table S4). Further investigation is required to confirm whether MLL fusions or the M5 subtype will be robust biomarkers of response to SLC5A3 repression in AML. Finally, we demonstrated the utility of dTAG-directed protein degradation for mimicking pharmacologic inhibition of the target, which is a valuable addition to AML target validation, especially for studying targets without a tool compound inhibitor available, such as SLC5A3 and MARCH5.

METHODS

Cell Culture and PDX Samples

All commercially available cell lines were obtained from ATCC or DSMZ. AML cell lines (MV4-11, U937, MOLM14, NB4, and P31FUJ) were cultured in RPMI supplemented with 10% FBS and 1% penicillin–streptomycin (PS). HEK293T cells were cultured in DMEM with 10% FBS and 1% PS. During the preparation of this study, *Mycoplasma* negativity was confirmed using a LookOut Mycoplasma PCR Detection Kit (MP0035; Sigma-Aldrich) and the identity of all cell lines was validated through short tandem repeat profiling by the Molecular Diagnostics Laboratory at the Dana-Farber Cancer Institute (DFCI). Details on myo-inositol depletion culture can be found in the Supplementary Methods.

Primary patient samples were acquired following written informed consent in accordance with the Declaration of Helsinki, and PDXs were established under protocols approved by DFCI and Cincinnati Children's Hospital Medical Center (CCHMC) Institutional Review Boards. The detailed information on PDXs is provided in Supplementary Table S1. For short-term *in vitro* culture, PDX cells were maintained in Iscove's modified Dulbecco's medium containing 20% FBS and 1% PS and supplemented with 10 ng/mL human SCF, TPO, FLT3L, IL3, and IL6 (300-07, 300-18, 300-19, 200-03, and 200-06; PeproTech).

Frozen $CD34^+$ HSPCs derived from bone marrow or umbilical cord blood were purchased from Lonza (#2M-101) and the Cell Processing Core at CCHMC, respectively. Details on nucleofection, genomic editing efficiency analysis, and colony formation assay can be found in the Supplementary Methods.

Lentivirus Production and Transduction

Details on lentiviral vectors used in this study can be found in the Supplementary Methods and Supplementary Table S5. Virus was produced using HEK293T cells transfected with lentiviral expression vectors, together with envelope VSVG and the gag-pol psPAX2 constructs. For transduction, AML cells were mixed with viral supernatant and 4 to 8 μg/mL polybrene. In some experiments, cells were centrifuged in viral supernatant at 1,000 × *g* for 1 hour at 33°C to enhance the transduction efficiency.

Competition Assay

Cells were transduced with lentivirus vectors coexpressing an sgRNA and a fluorescent protein, such as GFP, mCherry, or mAmetrine, at an efficiency of approximately 50%, or the transduced cells were mixed with nontransduced cells at approximately a 1:1 ratio. The cell growth was evaluated by the change in the fraction of cells expressing the fluorescent protein, which was monitored by flow cytometry. For the dTAG experiment, 500 nmol/L dTAG^V-1 was added into culture and replenished every 3 to 4 days.

Venetoclax Treatment

Venetoclax was acquired from Selleck (S8048) or MedChemExpress (HY-15531). Cells were plated in 384-well plates at 1,000 to 1,500 cells per well and mixed with serially diluted concentrations of venetoclax or 0.1% DMSO as a control. The viability of cells was measured after a 3-day incubation using a CellTiter-Glo Luminescent Cell Viability Assay kit (Promega) following the manufacturer's protocol. Data were analyzed using GraphPad Prism software (GraphPad Software).

Xenograft Transplantation

All animal experiments were approved by the DFCI and CCHMC Institutional Animal Care and Use Committees with adherence to all appropriate guidelines. Transplantation was performed on 6- to 8-week-old NOD/SCID/IL2RG$^{-/-}$ immunodeficient mice with transgenic expression of human SCF, GM-CSF, and IL3 (NSGS; The Jackson Laboratory). When necessary, mice were conditioned with sublethal irradiation at least 6 hours before transplantation. For doxycycline-inducible sg*MARCH5* experiments, 2×10^5 luciferase-expressing MV4-11 cells were transplanted into each mouse via tail vein. Doxycycline-containing food was initiated on day 4 posttransplantation. Leukemia progression was serially assessed using bioluminescence imaging. Mice were injected with 75 mg/kg i.p. d-Luciferin (Promega), anesthetized with 2% to 3% isoflurane, and imaged on an IVIS Spectrum (Caliper Life Sciences). A standardized region of interest encompassing the entire mouse was used to determine total bioluminescence flux. For the experiment evaluating venetoclax treatment in combination with *MARCH5* deletion, doxycycline-containing food was initiated on day 7 posttransplantation; 10 days postinjection, mice were treated with vehicle (60% Phosal 50 propylene glycol, 30% polyethyleneglycol 400, and 10% ethanol) or venetoclax (75 mg/kg body weight) daily by oral gavage for 1 week.

To establish the Cas9-PDX models, 0.5 to 2×10^6 AML PDX cells were transplanted. Engrafted cells were collected when mice displayed overt disease, and cells were sorted and retransplanted when needed. For doxycycline-inducible sg*SLC5A3* experiments, 5×10^5 PDX16-01 cells were transplanted into each mouse via tail vein, and doxycycline-containing food was initiated on day 7 posttransplantation. Leukemia progression was assessed by bone marrow aspiration 2 weeks afterward. For dTAG-MARCH5 experiments, 2×10^6 dTAG-MARCH5 PDX17-14 cells were transplanted into each mouse via tail vein. The treatment was initiated at 2 weeks (for the efficacy study) or 3 weeks (for the pharmacodynamic study) posttransplantation. dTAG^V-1 stock was prepared in DMSO, then a 1:20 dilution was made in saline solution containing 5% solutol, and the working solution was administrated via intraperitoneal or intravenous injection as indicated. Venetoclax was prepared as above. Details on flow cytometry analysis of leukemic engraftment and FKBP-HA-MARCH5 protein levels can be found in the Supplementary Methods.

In Vivo *and* In Vitro *Screens*

Screens were performed in duplicate. AML cells stably expressing Cas9 were transduced with the screen library at an efficiency of 30% to 50%, so that most cells received only one sgRNA. Puromycin selection was initiated on the day after transduction for 2 days, and the selected cells were recovered in fresh medium for 1 more day. On day 4 posttransduction, 1.5 million selected cells—sufficient for a representation of more than 1,000 cells per guide—were collected as the input reference. The remaining cells were divided into the *in vivo* and *in vitro* screens. For the *in vivo* screen, 10 million cells were transplanted into each sublethally irradiated NSGS mouse via tail vein, with four to five mice per replicate. Cells from mouse bone marrow and spleen were collected at around week 3 posttransplantation, when overt disease was observed. For the *in vitro* screens, at least 1.5 million cells were maintained throughout the 14- to 21-day culture period and collected at the end of the screen. Genomic DNA was extracted from collected cell pellets using a Qiagen DNeasy Blood and Tissue Kit (#69506) or a NucleoSpin Blood L kit (Takara #740954.20). The sgRNA barcodes were PCR amplified and submitted for standard Illumina sequencing, as previously described (4). The barcoding experiments were performed in a similar manner except using a barcoding library. Details on library construction and screen data analysis can be found in the Supplementary Methods.

Authors' Disclosures

S. Lin reports grants from the Leukemia & Lymphoma Society and NCI during the conduct of the study. B.K.A. Seong reports other support from Department of Defense (CA181249) during the conduct of the study. N.V. Dharia reports grants from St. Baldrick's Foundation during the conduct of the study, as well as other support from Genentech, Inc., a member of the Roche Group, outside the submitted work. J.A. Ryan reports personal fees from Zentalis outside the submitted work, as well as a patent for BH3 profiling issued to the Dana-Farber Cancer Institute and a patent for BH3 profiling licensed to Zentalis. F. Piccioni is a current employee of Merck Research Laboratories. L.H. Lee reports grants from St. Baldrick's Foundation during the conduct of the study. A. Letai reports personal fees from Zentalis Pharmaceuticals, Dialectic Therapeutitics, and Flash Therapeutics outside the submitted work, as well as patents related to BH3 profiling pending, issued, licensed, and with royalties paid to the Dana-Farber Cancer Institute. Dr. Letai and his lab get a fraction of the licensing fees. K. Stegmaier reports grants from the NCI, St. Baldrick's Foundation, and Children's Leukemia Research Association and other support from Cuban's Curing Childhood Cancer (4C's) during the conduct of the study, as well as personal fees from AstraZeneca, Bristol Myers Squibb, and Kronos Bio, personal fees and other support from Auron Therapeutics, and grants from Novartis outside the submitted work. No disclosures were reported by the other authors.

Authors' Contributions

S. Lin: Conceptualization, data curation, formal analysis, validation, investigation, visualization, methodology, writing–original draft, project administration. **C. Larrue:** Conceptualization, data curation, formal analysis, validation, investigation, visualization, methodology, writing–original draft, project administration. **N.K. Scheidegger:** Data curation, formal analysis, validation, investigation, writing–review and editing. **B.K.A. Seong:** Data curation, formal analysis, validation, investigation, methodology, writing–review and editing. **N.V. Dharia:** Software, formal analysis, investigation, visualization, methodology. **M. Kuljanin:** Data curation, formal analysis, investigation, visualization, methodology. **C.S. Wechsler:** Data curation, formal analysis, validation, investigation, visualization. **G. Kugener:** Software, investigation, methodology. **A.L. Robichaud:** Data curation, validation, investigation, methodology. **A.S. Conway:** Data curation, investigation, methodology. **T. Mashaka:** Data curation, formal analysis, investigation, visualization. **S. Mouche:** Data curation, validation, investigation. **B. Adane:** Data curation, validation, investigation, visualization. **J.A. Ryan:** Data curation, formal analysis, validation, investigation, visualization, methodology.

J.D. Mancias: Resources, supervision, investigation, writing–review and editing. **S.T. Younger:** Software, formal analysis, investigation, visualization, methodology. **F. Piccioni:** Software, formal analysis, investigation, visualization, methodology, writing–review and editing. **L.H. Lee:** Conceptualization, resources, data curation, formal analysis, investigation, methodology, writing–review and editing. **M. Wunderlich:** Conceptualization, resources, data curation, formal analysis, investigation, methodology, writing–review and editing. **A. Letai:** Resources, supervision, methodology. **J. Tamburini:** Conceptualization, resources, supervision, funding acquisition, investigation, visualization, methodology, writing–original draft, project administration. **K. Stegmaier:** Conceptualization, resources, supervision, funding acquisition, investigation, visualization, methodology, writing–original draft, project administration.

Acknowledgments

This work was supported by NCI R35 CA210030 (K. Stegmaier), P50 CA206963 (K. Stegmaier), R50 CA211404 (M. Wunderlich), and K99 CA263161 (S. Lin); the Children's Leukemia Research Association (K. Stegmaier); a St. Baldrick's Foundation Robert J. Arceci Innovation Award (K. Stegmaier); and the 4C's (K. Stegmaier). S. Lin is a Fellow of the Leukemia & Lymphoma Society. N.K. Scheidegger is supported by the Swiss Cancer League. B.K.A. Seong is supported by a Department of Defense PRCRP Horizon Award (CA181249). N.V. Dharia was supported by a St. Baldrick's Foundation Fellowship. L.H. Lee is a St. Baldrick's Foundation Scholar. The Flow Cytometry Core at the Cincinnati Children's Medical Center is supported by NIH S10OD023410.

The costs of publication of this article were defrayed in part by the payment of page charges. This article must therefore be hereby marked *advertisement* in accordance with 18 U.S.C. Section 1734 solely to indicate this fact.

Received December 23, 2020; revised July 26, 2021; accepted September 13, 2021; published first September 16, 2021.

REFERENCES

1. Ferrara F, Schiffer CA. Acute myeloid leukaemia in adults. Lancet 2013;381:484–95.
2. Wang T, Birsoy K, Hughes NW, Krupczak KM, Post Y, Wei JJ, et al. Identification and characterization of essential genes in the human genome. Science 2015;350:1096–101.
3. Hart T, Chandrashekhar M, Aregger M, Steinhart Z, Brown KR, MacLeod G, et al. High-resolution CRISPR screens reveal fitness genes and genotype-specific cancer liabilities. Cell 2015;163:1515–26.
4. Meyers RM, Bryan JG, McFarland JM, Weir BA, Sizemore AE, Xu H, et al. Computational correction of copy number effect improves specificity of CRISPR-Cas9 essentiality screens in cancer cells. Nat Genet 2017;49:1779–84.
5. Dempster JM, Pacini C, Pantel S, Behan FM, Green T, Krill-Burger J, et al. Agreement between two large pan-cancer CRISPR-Cas9 gene dependency datasets. Nat Commun 2019;10:5817.
6. Yamauchi T, Masuda T, Canver MC, Seiler M, Semba Y, Shboul M, et al. Genome-wide CRISPR-Cas9 screen identifies leukemia-specific dependence on a pre-mRNA metabolic pathway regulated by DCPS. Cancer Cell 2018;33:386–400.
7. Bajaj J, Hamilton M, Shima Y, Chambers K, Spinler K, Van Nostrand EL, et al. An in vivo genome-wide CRISPR screen identifies the RNA-binding protein Staufen2 as a key regulator of myeloid leukemia. Nature Cancer 2020;1:410–22.
8. Braun CJ, Bruno PM, Horlbeck MA, Gilbert LA, Weissman JS, Hemann MT. Versatile in vivo regulation of tumor phenotypes by dCas9-mediated transcriptional perturbation. Proc Natl Acad Sci U S A 2016;113:E3892–900.
9. Hidalgo M, Amant F, Biankin AV, Budinska E, Byrne AT, Caldas C, et al. Patient-derived xenograft models: an emerging platform for translational cancer research. Cancer Discov 2014;4:998–1013.
10. Townsend EC, Murakami MA, Christodoulou A, Christie AL, Koster J, DeSouza TA, et al. The public repository of xenografts enables discovery and randomized phase II-like trials in mice. Cancer Cell 2016;29:574–86.
11. Wang T, Yu H, Hughes NW, Liu B, Kendirli A, Klein K, et al. Gene Essentiality profiling reveals gene networks and synthetic lethal interactions with oncogenic Ras. Cell 2017;168:890–903.
12. McFarland JM, Ho ZV, Kugener G, Dempster JM, Montgomery PG, Bryan JG, et al. Improved estimation of cancer dependencies from large-scale RNAi screens using model-based normalization and data integration. Nat Commun 2018;9:4610.
13. Aguirre AJ, Meyers RM, Weir BA, Vazquez F, Zhang CZ, Ben-David U, et al. Genomic copy number dictates a gene-independent cell response to CRISPR/Cas9 targeting. Cancer Discov 2016;6:914–29.
14. Munoz DM, Cassiani PJ, Li L, Billy E, Korn JM, Jones MD, et al. CRISPR screens provide a comprehensive assessment of cancer vulnerabilities but generate false-positive hits for highly amplified genomic regions. Cancer Discov 2016;6:900–13.
15. Culp-Hill R, D'Alessandro A, Pietras EM. Extinguishing the embers: targeting AML metabolism. Trends Mol Med 2021;27:332–44.
16. Caino MC, Altieri DC. Molecular pathways: mitochondrial reprogramming in tumor progression and therapy. Clin Cancer Res 2016;22:540–5.
17. Xu Y, Milazzo JP, Somerville TDD, Tarumoto Y, Huang YH, Ostrander EL, et al. A TFIID-SAGA perturbation that targets MYB and suppresses acute myeloid leukemia. Cancer Cell 2018;33:13–28.
18. Tarumoto Y, Lin S, Wang J, Milazzo JP, Xu Y, Lu B, et al. Salt-inducible kinase inhibition suppresses acute myeloid leukemia progression in vivo. Blood 2020;135:56–70.
19. Lu B, Klingbeil O, Tarumoto Y, Somerville TDD, Huang YH, Wei Y, et al. A transcription factor addiction in leukemia imposed by the MLL promoter sequence. Cancer Cell 2018;34:970–81.
20. Hager K, Hazama A, Kwon HM, Loo DD, Handler JS, Wright EM. Kinetics and specificity of the renal Na+/myo-inositol cotransporter expressed in Xenopus oocytes. J Membr Biol 1995;143:103–13.
21. Nagashima S, Tokuyama T, Yonashiro R, Inatome R, Yanagi S. Roles of mitochondrial ubiquitin ligase MITOL/MARCH5 in mitochondrial dynamics and diseases. J Biochem 2014;155:273–9.
22. Aubrey BJ, Kelly GL, Kueh AJ, Brennan MS, O'Connor L, Milla L, et al. An inducible lentiviral guide RNA platform enables the identification of tumor-essential genes and tumor-promoting mutations in vivo. Cell Rep 2015;10:1422–32.
23. Chau JF, Lee MK, Law JW, Chung SK, Chung SS. Sodium/myo-inositol cotransporter-1 is essential for the development and function of the peripheral nerves. FASEB J 2005;19:1887–9.
24. Phelps DL, Ward RM, Williams RL, Nolen TL, Watterberg KL, Oh W, et al. Safety and pharmacokinetics of multiple dose myo-inositol in preterm infants. Pediatr Res 2016;80:209–17.
25. Chatree S, Thongmaen N, Tantivejkul K, Sitticharoon C, Vucenik I. Role of inositols and inositol phosphates in energy metabolism. Molecules 2020;25:5079.
26. Chen Z, Liu L, Cheng Q, Li Y, Wu H, Zhang W, et al. Mitochondrial E3 ligase MARCH5 regulates FUNDC1 to fine-tune hypoxic mitophagy. EMBO Rep 2017;18:495–509.
27. Xu S, Cherok E, Das S, Li S, Roelofs BA, Ge SX, et al. Mitochondrial E3 ubiquitin ligase MARCH5 controls mitochondrial fission and cell sensitivity to stress-induced apoptosis through regulation of MiD49 protein. Mol Biol Cell 2016;27:349–59.
28. Nabet B, Ferguson FM, Seong BKA, Kuljanin M, Leggett AL, Mohardt ML, et al. Rapid and direct control of target protein levels with VHL-recruiting dTAG molecules. Nat Commun 2020;11:4687.
29. Ni Chonghaile T, Sarosiek KA, Vo TT, Ryan JA, Tammareddi A, Moore Vdel G, et al. Pretreatment mitochondrial priming correlates with clinical response to cytotoxic chemotherapy. Science 2011;334:1129–33.

30. Vogler M, Walter HS, Dyer MJS. Targeting anti-apoptotic BCL2 family proteins in haematological malignancies - from pathogenesis to treatment. Br J Haematol 2017;178:364–79.
31. Djajawi TM, Liu L, Gong JN, Huang AS, Luo MJ, Xu Z, et al. MARCH5 requires MTCH2 to coordinate proteasomal turnover of the MCL1:NOXA complex. Cell Death Differ 2020;27:2484–99.
32. Haschka MD, Karbon G, Soratroi C, O'Neill KL, Luo X, Villunger A. MARCH5-dependent degradation of MCL1/NOXA complexes defines susceptibility to antimitotic drug treatment. Cell Death Differ 2020; 27:2297–312.
33. Subramanian A, Andronache A, Li YC, Wade M. Inhibition of MARCH5 ubiquitin ligase abrogates MCL1-dependent resistance to BH3 mimetics via NOXA. Oncotarget 2016;7:15986–6002.
34. Arai S, Varkaris A, Nouri M, Chen S, Xie L, Balk SP. MARCH5 mediates NOXA-dependent MCL1 degradation driven by kinase inhibitors and integrated stress response activation. Elife 2020;9:e54954.
35. DiNardo CD, Pratz K, Pullarkat V, Jonas BA, Arellano M, Becker PS, et al. Venetoclax combined with decitabine or azacitidine in treatment-naive, elderly patients with acute myeloid leukemia. Blood 2019;133:7–17.
36. Pan R, Hogdal LJ, Benito JM, Bucci D, Han L, Borthakur G, et al. Selective BCL-2 inhibition by ABT-199 causes on-target cell death in acute myeloid leukemia. Cancer Discov 2014;4:362–75.
37. Jin S, Cojocari D, Purkal JJ, Popovic R, Talaty NN, Xiao Y, et al. 5-Azacitidine induces NOXA to prime AML cells for venetoclax-mediated apoptosis. Clin Cancer Res 2020;26:3371–83.
38. Pearce DJ, Taussig D, Zibara K, Smith LL, Ridler CM, Preudhomme C, et al. AML engraftment in the NOD/SCID assay reflects the outcome of AML: implications for our understanding of the heterogeneity of AML. Blood 2006;107:1166–73.
39. Pikman Y, Puissant A, Alexe G, Furman A, Chen LM, Frumm SM, et al. Targeting MTHFD2 in acute myeloid leukemia. J Exp Med 2016; 213:1285–306.
40. Jones CL, Stevens BM, D'Alessandro A, Reisz JA, Culp-Hill R, Nemkov T, et al. Inhibition of amino acid metabolism selectively targets human leukemia stem cells. Cancer Cell 2018;34:724–40.
41. Shibazaki T, Tomae M, Ishikawa-Takemura Y, Fushimi N, Itoh F, Yamada M, et al. KGA-2727, a novel selective inhibitor of a high-affinity sodium glucose cotransporter (SGLT1), exhibits antidiabetic efficacy in rodent models. J Pharmacol Exp Ther 2012;342:288–96.
42. Meng W, Ellsworth BA, Nirschl AA, McCann PJ, Patel M, Girotra RN, et al. Discovery of dapagliflozin: a potent, selective renal sodium-dependent glucose cotransporter 2 (SGLT2) inhibitor for the treatment of type 2 diabetes. J Med Chem 2008;51:1145–9.
43. Park YY, Nguyen OT, Kang H, Cho H. MARCH5-mediated quality control on acetylated Mfn1 facilitates mitochondrial homeostasis and cell survival. Cell Death Dis 2014;5:e1172.
44. Takeda K, Nagashima S, Shiiba I, Uda A, Tokuyama T, Ito N, et al. MITOL prevents ER stress-induced apoptosis by IRE1alpha ubiquitylation at ER-mitochondria contact sites. EMBO J 2019;38:e100999.
45. Yoo YS, Park YY, Kim JH, Cho H, Kim SH, Lee HS, et al. The mitochondrial ubiquitin ligase MARCH5 resolves MAVS aggregates during antiviral signalling. Nat Commun 2015;6:7910.
46. Sharon D, Cathelin S, Mirali S, Di Trani JM, Yanofsky DJ, Keon KA, et al. Inhibition of mitochondrial translation overcomes venetoclax resistance in AML through activation of the integrated stress response. Sci Transl Med 2019;11:eaax2863.
47. Chen X, Glytsou C, Zhou H, Narang S, Reyna DE, Lopez A, et al. Targeting mitochondrial structure sensitizes acute myeloid leukemia to venetoclax treatment. Cancer Discov 2019;9:890–909.
48. Burgess A, Chia KM, Haupt S, Thomas D, Haupt Y, Lim E. Clinical overview of MDM2/X-targeted therapies. Front Oncol 2016;6:7.
49. Boddu P, Carter BZ, Verstovsek S, Pemmaraju N. SMAC mimetics as potential cancer therapeutics in myeloid malignancies. Br J Haematol 2019;185:219–31.